Chapter 9

Eulerian-Style Measurements Incorporating Nonmechanical Sensors

Chapter Outline

Understanding the dynamics of a number of important ocean processes, such as frontogenesis, mixed-layer evolution, inertial-interval wave generation, and coastal/shelf wave development, requires long-term (weeks to years) high-resolution (meters to tens of meters vertically, hundreds of meters to kilometers horizontally) measurement of the three-dimensional velocity field in the frequency band from 0 to 1 Hz. There are also fine and microstructures in the ocean current regime; therefore, sensors used for studies of such currents must respond fast enough to follow most of the high-frequency components in the flow signal and must be sensitive enough to detect minute variations in the flow field. Measurements of low-frequency, small-amplitude mean currents in the presence of turbulent currents as well as surface wave- or internal wave-induced orbital currents also require sensitive sensors. Nonmechanical speed and direction sensors best satisfy the required frequency response and ruggedness criteria. Purely mechanical sensors' inherent limitations, such as high thresholds, poor high-speed endurance, poor sensitivities, and limited frequency response, render rather difficult the measurement of very weak and very strong currents as well as high-frequency constituents that are present in the surface wave-induced or internal wave-induced orbital currents.

These limitations of mechanical sensors led to the development of rapid-responding nonmechanical sensors. Collective efforts expended by several technologists led to the successful implementation of such sensors into the subsequent generation of current meters. Thus, over a period of time, Eulerian-style measurement methods gradually progressed from those relying on purely mechanical sensors to those incorporating advanced electromechanical, acoustic, laser, and thermal sensors. These efforts resulted in the availability of highly sensitive sensors for measurements in turbulent current regimes and, in turn, stimulated the oceanographers to undertake fine-scale measurements that were not possible before for lack of suitable instrumentation. In situations in which high-frequency processes need to be examined, these specialized sensors' output can be sampled rapidly enough in time to match the processes of interest. Where low-frequency processes are to be studied, the averaging time can be chosen appropriate to the type of motions involved.

This chapter addresses three types of nonmechanical sensor: electromagnetic (EM) sensors, acoustic travel-time (ATT) difference sensors, and acoustic Doppler (AD) sensor.

9.1. ELECTROMAGNETIC SENSORS

EM sensors have been used for several decades for measurement of water flows in open water bodies such as oceans, lakes, and rivers as well as in constrained environments such as pipes. The basic principle dates from the days of Faraday. The EM current meter was developed and has been used for a number of years by the Institute of Oceanographic Sciences, Wormley, England. In the 1950s it was employed to measure turbulent fluctuations in tidal currents in the Irish Sea (Bowden and Fairbairn, 1956). Subsequently, it was developed as a ship's log, and Tucker et al. (1970) described its use for this purpose and its

Measuring Ocean Currents. http://dx.doi.org/10.1016/B978-0-12-415990-7.00009-0

principle of operation. As a current meter it has several advantages over more conventional devices. Its output is linear down to zero flow and independent of temperature, salinity, and pressure. It has no moving parts and is not particularly prone to damage during launching operations nor to fouling or corrosion. Use of two orthogonal pairs of electrodes permits simultaneous measurement of two orthogonal components of flow signals and therefore avoids the need for a current direction-orienting vane.

EM current meters also have the advantage of having high sensitivity, excellent linearity, and good directional response but no moving parts (Olson, 1972). They can measure two components of water current; this property may be useful, for example, if Reynolds stresses are to be measured (Thorpe et al., 1973). An EM sensor also possesses large linear dynamic range and excellent dynamic response and keeps a constant calibration. Kanwisher et al. (1975) reported an interesting example to illustrate the rapid dynamic response of EM sensors. In an EM sensor, the electrical output changes sign with the change in direction of the water current. This means that a moored EM current meter, unlike a Savonius rotor current meter, will not tend to produce a net output as a result of "rectification" of apparent currents in response to pumping motions.

The theory of EM current meters belongs to the subject of magneto-hydrodynamics, formed by the combination of the classical disciplines of fluid mechanics and electromagnetism (Shercliff, 1962; Bevir, 1970). Fluid moving in a magnetic field experiences electromotive force acting in a direction perpendicular to both the motion and the magnetic field. According to Faraday's principle of electromagnetic induction (EMI), an electrical potential gradient is developed across any conductor that moves perpendicularly through a magnetic field (see Figure 9.1). The magnitude of this potential gradient (E) depends on the magnetic flux density (B), the conductor velocity (V), and the conductor length (L), according to the relationship:

$$U = (V \times B)L \tag{9.1}$$

Thus, for any constant B and L, the potential gradient (U) across the conductor is directly proportional to the conductor velocity, V. When Faraday's principle is employed for water current measurements, the "conductor" is the water. Fortunately, the river and ocean waters possess sufficient conductivity to permit the use of the EMI principle for water current measurements. Apart from the primary application of EM current meters for measurement of motional velocities of electrical conducting fluids, there are several potential applications for EM flow sensors in industrially important multiphase flows in which the continuous phase has a relatively high electrical conductivity (e.g., water) whereas the dispersed phase or phases have a much lower conductivity. These include (1) "rock particle in water" flows that occur during the hydraulic transportation of rock in mineral-processing applications; (2) "rock cuttings in water-based drilling mud" flows that occur during oil-well drilling operations; (3) oil-in-water flows that occur down-hole in offshore oil wells at pressures that are too great to allow dissolved gases to come out of solution; (4) oil-and-gas-in-water flows that can occur at the wellhead in oil production operations, and (5) solids-in-water flows that occur in wastewater treatment applications (Wang et al., 2007). It has also been shown that in vertical, bubbly gas-water flows, EM flow meters can be used to measure the mean velocity of the water (Bernier and Brennen, 1983). These characteristics of EM flow meters render them suitable for current measurements in the surf zone of the oceans, where the seawater is often impregnated with air bubbles and minute sand particles thrown by the breaking waves.

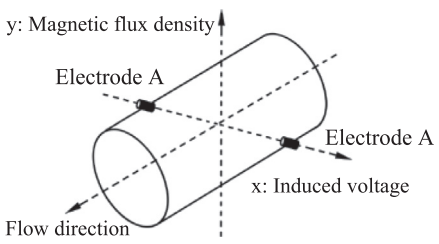

FIGURE 9.1 Geometry illustrating the principle of electromagnetic flow meters. *(Source: Wang et al., 2007.)*

After some assumptions were made, Shercliff (1962) proposed a weight function that describes the contribution of different parts of the EM flow meter measurement to the total signal. This function shows that the effect of velocity is strong near the electrodes and decreases when moving further away from the electrodes. The weight function therefore describes spatial variations in the EM flow sensor's sensitivity, which is a function of the magnetic flux density and the size, shape, and positions of the electrodes. According to Shercliff's weight function, the induced voltage across the electrode pair can be expressed as follows (Shercliff, 1962):

$$U = \frac{2a}{\pi a^2} \iint B(x,y)v(x,y)W(x,y)dxdy \tag{9.2}$$

where U is the induced voltage when the electrode pair is located at various positions (x, y), B is the magnetic flux density, v is the flow velocity at each point of the flow region in the cross-section of the flow channel bounded by the magnetic field, W is the "weight" value at each point of the flow region in the cross-section of the flow channel bounded by the magnetic field, and a is the radius of the circular cross-section bounded by the magnetic field. Wang et al. (2007) reported a numerical approach to the determination of EM flow meter weight functions. Although the induced voltage is "conductivity-weighted," laboratory

experiments have shown (Olson, 1972; Sanford et al., 1975) that changes in "zero" (i.e., output in the absence of currents) and sensitivity due to water composition changes can be neglected in circumstances in which the electrode separation (L) is not appreciably large.

EM sensors employed for detection of ocean currents can broadly be categorized into two classes according to the source of the magnetic field used to detect the water-motion signal: (1) those that utilize the Earth's magnetic field, and (2) those that locally generate their own magnetic field. Eulerian-style EM current meters fall under the latter category.

9.1.1. Electromagnetic Current Meters

In the design of EM current meters meant for Eulerian-style current measurements, the geomagnetic electro kinetograph (GEK) method mentioned in Chapter 2 was modified to generate a sufficiently strong local magnetic field using a coil that functions as an electromagnet. Uniformly distributed local magnetic field (i.e., homogeneous magnetic field) can be created using a pair of Helmholtz coils. Helmholtz coils are usually used as the excitation coils in the design of EM flow meters intended for measurement of fluid flows through large pipes, wherein the flow velocity away from the axis of the pipe decreases with increasing distance from the pipe's axis because of boundary effects imposed by the wall of the pipe. A Helmholtz coil consists of a parallel pair of identical circular coils spaced one radius apart and wound so that the electrical current used for exciting the coils flows through both coils in the same direction. This winding results in a uniform magnetic flux density between the coils, with the primary component parallel to the common axes of the two coils.

The material of Helmholtz coils is copper. Based on measurements using a magnetic camera, consisting of a rectangular array of closely spaced Hall sensors, Wang et al. (2008) experimentally demonstrated that Helmholtz coils generate uniform magnetic flux density. From Equation 9.2, a uniform magnetic flux density simplifies the computation of water current flow velocity based on induced voltage measured by the data acquisition system. Figure 9.2 shows a typical example of the placement of the Helmholtz coils used with a flow meter for water pipes, together with the orientation of the magnetic field generated by the Helmholtz coil, positioning of electrode pairs, and the water flow-induced voltages.

For logistic reasons, current meters need to be small in size, and therefore the sensor of an EM current meter must also be small in size. This requirement calls for the use of a multiturn single-coil bunch rather than a pair of Helmholtz coils for generation of a strong magnetic field. A pair or pairs of electrodes situated within this relatively strong

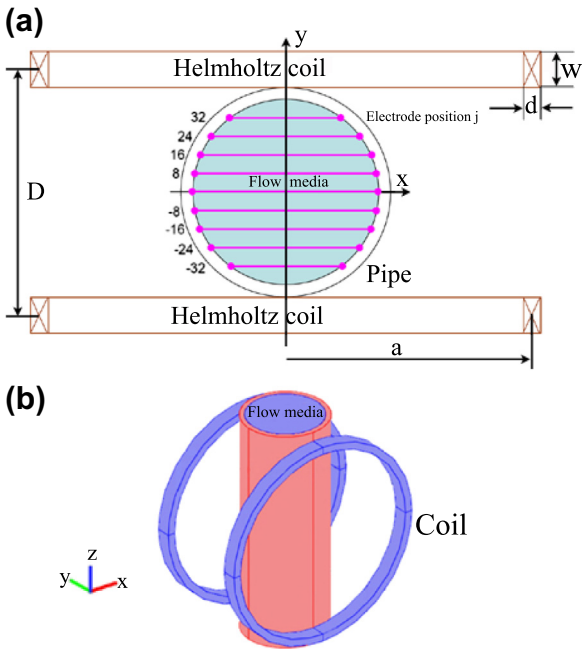

FIGURE 9.2 A typical example of the placement of Helmholtz coils used for flow measurements in pipes. *(Source: Wang et al., 2008.)*

magnetic field give rise to measurable potentials with small (less than 10 cm) electrode separation. Thus, in this type of EM current meter, the magnetic field is impressed on the water using a multiturn coil buried in the sensing head.

EM current meters are usually configured for measurement of two mutually orthogonal horizontal current components. In this case, measurements of the potential gradients are made from two orthogonally mounted pairs of electrodes. A steady direct current (DC) could be used to drive the Helmholtz coils, resulting in a steady, nonvarying magnetic field. However, this technique would superimpose the resulting microvolt-level DC signal voltage (i.e., flow-induced potential gradient across the electrodes) on the wideband electrical noise generated from a variety of sources such as electrochemical actions at the electrode surface, variable polarization potentials at the electrodes, and stray DC potentials in the water. In the case of ocean currents, the electrochemical voltages generated at the measuring electrodes are typically 10−1,000 times larger than the water-motion-induced voltages (McCullough, 1980). Consequently, it would be very difficult to accurately detect a DC signal; therefore, this calls for some sort of frequency separation of the low-frequency electrochemically induced voltages. As a result, most designs of local magnetic field type EM current meters drive the electromagnet with an alternating current (AC) or switched DC, thereby creating an alternating signal (voltage) of known frequency. Furthermore, application of an alternating magnetic field permits drift-free amplification of the microvolt-level alternating potential generated

across the electrodes and largely reduces long-period noise and electrode effects. Because the magnetic field is modulated at a higher frequency relative to the undesired electrode potential variations, synchronous detection of the water-current-induced voltage signal becomes possible. This technique greatly simplifies the instrument design. Practical designs typically evolve from sinusoidal to chopped-DC excitation.

The water current flow field in the immediate vicinity of a sensor head, established to a large extent by the head geometry, is of critical importance in that it determines the degree of linearity that can be achieved as well as the nature of the directional response. Characteristics of the flow that are important include the thickness and velocity dependence of the surface boundary layer, especially in the proximity of the embedded electrodes, as well as the existence of flow separation effects that create complex flows capable of generating substantial nonlinearity in the sensor output. Modeling techniques, when applied to flow conditions and sensor response, can provide a basis for understanding sensor behavior and for prediction when seeking an optimum head design (Collar, 1993). Cushing (1976) constructed analytical models in order to compare the responses of different head geometries.

Forms of head shape that have been considered or used include "open" electrode configuration and various solids of revolution, such as spheres, cylinders, and ellipsoids (Figure 9.3). Although the hydrodynamic performance weighs heavily in choice of shape, this may be balanced in individual cases by considerations such as ease of fabrication and durability.

EM current meters of initial designs employed an "open" electrode configuration (Olson, 1972). This scheme minimizes the disturbance to the flow as far as is practicable. This approach has been adopted at the National

FIGURE 9.3 Samples of some electromagnetic sensors incorporated in electromagnetic current meters. *(Source: Valeport brochure; reproduced with kind permission of Kevin Edwards, Sales and Marketing Manager, Valeport Ltd., UK.)*

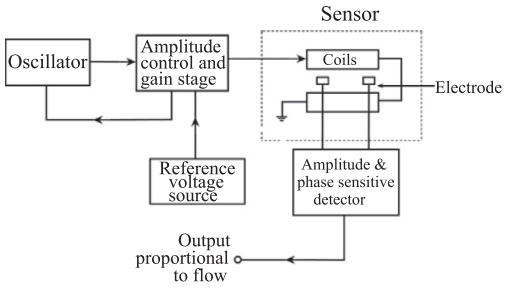

FIGURE 9.4 Block diagram of a conventional electromagnetic flow meter system. *(Source: Desa and Desa, 1980.)*

Institute of Oceanography (NIO) in India (Desa and Desa, 1980; Joseph, 1981) and Institute of Oceanographic Sciences (IOS) in the United Kingdom in work on the measurement of mean current in the wave zone (Collar, 1993). A block diagram of the conventional electromagnetic flow meter system is shown in Figure 9.4. In this flow meter, a pair of Helmholtz coils is driven by a low-frequency sinusoidal current. The induced flow signal is sensed by two electrodes located in the plane midway between the two coils. In operation, the output of a Wien bridge oscillator is passed through a fixed gain stage, and thence to a driver, which powers the coils. The electrode output is sensed by a field effect transistor (FET) input instrumentation amplifier (a near-ideal differential amplifier). The output contains both the flow signal and the induced quadrature voltages. The quadrature voltages are cancelled by adjusting the phase-sensitive detector waveform to sample equal amounts of positive and negative excursions of the quadrature signal. The remaining flow signal is also fed to the detector, which averages out noise and other unwanted signals. The detector consists of an FET switch by a suitably phased signal derived from the driver. The FET output is coupled to a buffer amplifier for transmission and display. The output of the detector is linearly related to the water flow velocity. This EM current meter was tested in a freshwater tow tank of dimensions 213 m $\times$ 3.6 m $\times$ 2.7 m. The results are shown in Figure 9.5. A root-mean-square (rms) deviation of 0.009 m/s

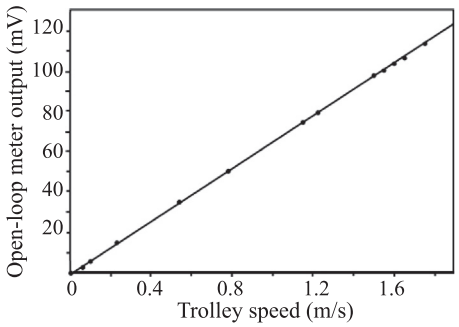

FIGURE 9.5 Calibration curve of a conventional EM current meter output with trolley velocity. *(Source: Desa and Desa, 1980.)*

over a range from 0.06 to 1.96 m/s (a factor of approximately 33) was obtained.

A flexible configuration of a variant of the open electrode configuration for an array of sensors has been developed by Sorrell et al. (1990) for measurements in energetic regions of the ocean where the current flow has high spatial and temporal variability. Central to the system is a two-axis EM current meter that measures the water current flow through a ducted volume containing a uniform magnetic field and nonprotruding electrodes flush with the duct surfaces. This geometry minimizes the electrode boundary-layer effect on the output, thus improving calibration and reducing fouling and damage potential. A patented inexpensive amplifier for low S/N ratios is employed to produce very low "zero drift" during operation. Electromagnetic sensors in various compact configurations have been fabricated previously, and many have worked acceptably. A central problem with this type of sensor has been the inherently low induced-output voltage, when power is limited for magnetic field generation. The low S/N ratio necessitates high-gain amplification, leading to problems with zero drift. In addition, the voltage signal-sensing electrodes have inherent, transient, electrochemical potential differences as well as other types of potential differences related to local boundary layer development/destruction. The relatively slow drifting electrochemical differences can be effectively eliminated by AC driving the magnetic field generating coil. The boundary layer-related differences can be controlled by physical isolation of the electrodes from the flow and/or with the use of geometry with reproducible boundary layer effects related to the flow-field measurement volume.

In the EM sensor reported by Sorrell et al. (1990), two improvements address the criteria of low zero drift and good high frequency as well as angular response on and off axis. First, a new low-cost amplifier circuit was designed for low S/N ratio and a high common mode rejection ratio (CMRR), thus providing very low zero drift. Second, a better geometric configuration (i.e., silver-silver chloride electrodes mounted flush in the face of the coil housing) was developed to control boundary layer and fouling problems as well as improve ruggedness and deployment flexibility. The magnetic field is generated by a Helmholtz coil arrangement, as reported by Olson (1972); however, the electrodes and coils are configured differently. For example, the coil units are solid rather than open, thus providing a ducted flow measurement volume within a highly uniform field. Identical sets of electrodes are flush-mounted on opposing faces of the sensor (coplanar with the coils) and connected in parallel. The complete configuration is mechanically robust, hydrodynamically clean, and symmetric, providing reliable precision measurements.

The electrodes have diameter of 2 mm, and two pairs of electrodes are located at 90° to each other. Each component of the water flow velocity is measured by the two electrodes; the axis connecting them is perpendicular to the flow. By locating two sets of electrodes 90° to each other (i.e., orthogonally), the velocity components 90° to each other can be measured. To average the flow velocity in the flow-sensing volume, electrode pairs are located in both the top and bottom coil housing. These electrode pairs provide two sources of induced voltage output, and the output from the pairs is averaged. An electrode located at the center of each coil housing is used to establish an "electrical signal ground" for the electronics. This arrangement of the electrodes not only averages the induced voltage over the flow-sensing volume, but it also provides redundancy if one of the two pairs of electrodes is damaged or fouled. The interior location of the electrodes minimizes the likelihood of biological fouling or mechanical damage from external impact.

The coil housings are held in place by a support structure, which consists of a hub over each coil housing connected by a support frame of four tubular members. One of the tubular frame members can be removed for access to the coil housings. Each coil housing can be removed individually from the structure. For shallow-water applications, the sensor is attached to the mooring by plastic piping that fits over the support hub. The pipe is attached to the hub by a locking ring and sealed with O-rings. The electronics for each sensor can be housed in a sealed portion of the mooring pipe, next to the sensor. Another alternative is to run electrical cables through the mooring pipe and the tubular support members. The usual practice is to locate the amplifier electronics next to each sensor and cable the output from several sensors in an individual mooring to a central power supply/data logger/compass unit located at the bottom of the mooring. The tubular support members are specifically designed to be large enough in internal diameter to carry all the cables necessary for most applications. With this flexibility in electronic component location, and because the sensor is an integral load carrying part of the mooring, the sensors can be configured as a vertical array. The sensors can also be electronically connected to common components or used as a single-point mooring. In situations where a number of closely spaced sensors are needed, such as in boundary layer phenomena, several of them can be located in a vertical array.

The sensor electronics supplies a stabilized square-wave excitation to the Helmholtz coil system. A synchronous demodulation system is then used to measure the flow-induced voltage signal. The square-wave frequency is maintained accurately at 15 Hz to cancel the large amounts of 60-Hz interference often encountered in the tow tanks used for calibration. The high-gain front-end amplifier uses low-noise operational amplifiers configured into a unique differential scheme. The circuit is specifically designed for the decoupling of both DC and low-frequency electrode

offset potentials due to galvanic electrochemistry, noise, or other sources. A capacitor is used in the feedback loop to decouple DC and low-frequency voltage offset on the electrodes. Sorrell et al. (1990) used this patented scheme (Sorrell et al., 1985) in place of the usual method of AC coupling of the electrodes to the amplifiers. It has the advantage of giving high common-mode rejection when the electrical characteristics of the electrodes are not identical. This advantage is missing with direct AC coupling. Two such differential amplifiers are employed in a cascade to permit high gain with good bandwidth and minimum phase errors.

The synchronous demodulator uses a refractory period after each transition of the coil excitation for magnetic field generation. This scheme permits the coil current to stabilize and allows the large electrical transients, which result from the high rate of change of the magnetic field, to decay. Sorrell et al. (1990) observed that these transients are more pronounced in the presence of boundaries that disturb the magnetic field symmetry. Therefore, for example, these transients tend to be larger near the wall in a tow tank. The modulator samples the amplified signal only during the second half of each magnetic field phase. Signal conditioning for the resulting demodulated flow signal varies with the specific application. For the near-shore applications, which have a measurable surface gravity-wave (wind-generated wave) velocity component, the signal is filtered by a second-order Butterworth filter, usually having a 3-dB roll-off at 1 Hz.

As noted in Chapter 8, the performance of current meters needs to be established based on the results of tow-tank tests and field intercomparison studies. Sorrell et al. (1990) conducted all tow-tank tests in the Environmental Protection Agency's (EPA) Fluid Modeling Facility. Calibration of their EM sensor was carried out by mounting the sensor on the carriage of the tow tank and then towing the carriage down the tank at a number of selected constant towing speeds. The results of the test show that the sensor's output is essentially linear over the entire range of carriage speeds (the maximum carriage speed possible was 49 cm/s), with an rms error (in speed) of 0.3 cm/s. The maximum percent error in speed was 4%, with an average error of 2%. The range of testing not only indicated the proper operation of the sensor electronics but also lent confidence that changes in the boundary layer over the electrodes, for the speed range investigated, did not alter the linear response of the sensor.

A series of detailed tests on the angular response of the EM sensor was carried out by Sorrell et al. (1990) by repeating the full-calibration tests by rotating the sensor in normal attitude through various selected measured positive and negative horizontal azimuthal angles. The test results show that the sensor output is slightly higher at negative horizontal azimuthal angles than at positive angles. The reason for the observed difference in the azimuthal angular response has been attributed to the sensor's misalignment at the start of the angular response tests. However, the azimuthal response is reasonably consistent and, therefore, reduction of data to determine the flow angle should be straightforward.

Sorrell et al. (1990) conducted dynamic response tests by mounting a mechanical oscillating device on the carriage. The oscillator was driven by a Scotch yoke driver, which was intended to produce an oscillating horizontal motion with a single harmonic component. The sensor was mounted on a string attached to the mechanism, and the entire system is referred to as an *oscillating arm*. The arm position was measured with a linear displacement transducer. The arm position was then differentiated to yield the arm velocity. This was then added to the carriage velocity to provide the instantaneous sensor velocity. The sensor was mounted with one axis parallel (parallel channel) to the flow motion and the other axis perpendicular (cross channel) to the flow. Output from both sensor channels and the oscillating arm position was digitally sampled at 0.01-s intervals. In each individual test, a total of 2,048 data points were recorded for each channel. The conditions for these tests were a mean flow (carriage) velocity of 30.7 cm/s and a maximum oscillatory velocity of 44 cm/s with a frequency of approximately 1 Hz. This is a relatively severe test in that the sensor is subjected to a high-frequency (1 Hz) unsteady flow and to both positive and negative velocities. Output from the parallel channel of the sensor indicates good dynamic response at frequencies of 1 Hz. The cross-channel output exhibits a higher frequency oscillation component. This component becomes quite large at the time when the oscillating arm has a relatively large deviation from single-frequency harmonic motion (referred to as a *jerk* in the arm motion). Similar higher-frequency oscillations were observed in both the parallel-channel and the cross-channel outputs when the sting was visually observed to vibrate. The frequency of these higher oscillations was found to be at approximately the natural frequency of the sting, which adds to the belief that they are due to the sting vibration. The higher-frequency oscillations in the cross-channel output did not average to zero, which is believed to be due to slight misalignment of the cross-channel axis with the flow motion (i.e., the cross-channel is not exactly perpendicular to the arm plus carriage flow motion).

Often, in the unsteady flows of interest, the flow velocity is not confined to two dimensions. The EM current sensor developed by Sorrell et al. (1990) is designed to measure two planar-flow components that are typically, but not necessarily, in the horizontal plane. To be able to do this, it is important that any flow component that is in the third dimension, or "out-of-plane" for a particular sensor orientation, not alter or contaminate the "in-plane" measurement. A flow component at an angle α should not

alter the flow in the plane of the sensor housings. To investigate this idea, the entire sensor and the semi-rigid mooring pipe on which it was attached were mounted at an angle of 45° to the vertical. The sensor, so inclined, was then oscillated and translated horizontally down the tank, as in the prior tests. This produced a flow component that was inclined 45° to the sensor, or $\alpha = 45°$. Thus, in this dynamic response test, the flow was 45° out of plane of the sensor, i.e., with the sensor inclined at an angle of 45° to the vertical. The sensor's dynamic response (i.e., its tilt response) at high angle of flow inclination (45°) appears to be encouraging.

In addition to the extensive steady-state flow-calibration tests and dynamic tests of the EM sensor in the tow tank, which demonstrated its linear response over a moderate range of velocities and its reasonably good cosine angular response, Sorrell et al. (1990) reported separate *in situ* tests. In one of these tests, the sensor was installed from a bridge in an estuary. The flow had few dynamic characteristics that challenged the sensor's response characteristics, but the situation tested the sensor's long-term reliability. Data were collected for a period of over a year, indicating the sensor's reliability under field conditions for at least this long. The sensor required no maintenance during the entire year, but by the end of the year the sensor had become so biologically fouled that there was partial blockage of the flow sensor volume.

It was shown that the EM sensor has a sufficiently good dynamic response so that the high-frequency parameters of even the highly unsteady oceanic flows can be accurately measured, even in relatively severe environments. In addition, the sensor was found to maintain linear response and low zero drift required to accurately measure the mean flow properties.

As indicated earlier, the EM sensors have undergone several development phases. The drawback of an increase of noise level due to vortex shedding from the Helmhotz coils and their supports employed in the "open" electrode configuration necessitated alternate sensor designs. An ellipsoidal "head" is a result of such design initiatives. For example, the EM current meter designed by Thorpe et al. (1973) consists of an energizing coil with a vertical axis (Figure 9.6), which is encapsulated in an ellipsoidal head. The electrical current passing through the coil produces a magnetic field. Conducting seawater moving through the magnetic field produces a potential voltage gradient at right angles to both the magnetic field and the direction of seawater flow, and this is sensed by two pairs of electrodes mounted on the face of the head. The voltage ratios bear a direct relationship to the horizontal direction of the water flow past the head. Electrochemical effects associated with DC and direct electromagnetic and capacitive coupling induced by AC are avoided by driving the coil by a switched DC. A steady current (governed by the switched DC coil-excitation voltage waveform) is passed through the coil and, after a fixed interval of time to cover the decay of transients, the amplified voltages from each pair of electrodes are briefly switched to storage capacitors. The current passing through the coil is then reversed (again governed by the switched DC coil-excitation voltage waveform) and the process is repeated using second capacitors. The potential difference between the two pairs of stored voltage levels is then a direct measure of water current speeds normal to the two pairs of electrodes.

The sensing head (Figure 9.7) used by Thorpe et al. (1973) is based on the design described by Tucker et al. (1970) for the ship's log and consists of a bifilar wound energizing coil and four electrodes contained in a solid epoxy resin molding with a maximum external diameter of 11.2 cm. Considerable research has been done to obtain the

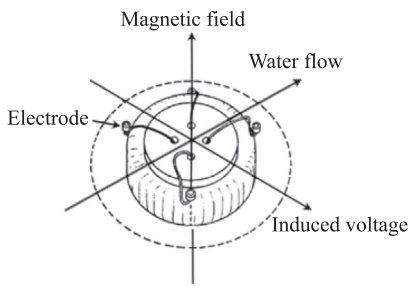

FIGURE 9.6 An EM sensor's bifilar wound resin-impregnated energizing coil and two pairs of electrodes across which water-flow-induced potential voltage gradients are generated. *(Source: Thorpe et al., 1973.)*

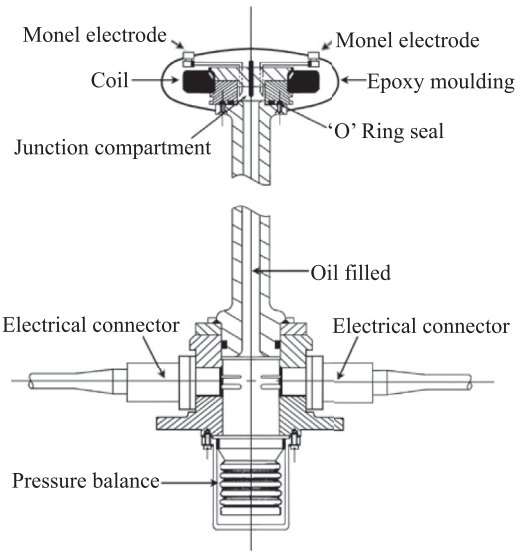

FIGURE 9.7 The cross-section of the sensing head of an EM current meter sensor, which consists of a bifilar wound resin-impregnated energizing coil and four electrodes contained in a solid epoxy resin molding. The supporting strut and the junction compartment at the back of the head are filled with oil and pressure-balanced by means of a diaphragm. *(Source: Thorpe et al., 1973.)*

best configuration for the coil and electrodes and for the shape of the head. For example, the existing sensors were found to contain coils with an air gap between the windings, which inevitably resulted in a collapse of the outer molding when the sensor was subjected to high pressures, and new heads were therefore made with resin-impregnated coils to overcome this problem. Stresses on the head were further reduced by filling the supporting strut and the junction compartment at the back of the head with oil and pressure-balancing this by means of a diaphragm. This oil filling also helped with the insulation of the leads where they emerge from the head casting in the junction compartment. The head has been tested hydrostatically to a depth of 3,000 m.

Figure 9.8 shows the assembled instrument. The sensing head (A) with the plane of the coil horizontal is mounted on the supporting strut (B) 55 cm above the aluminium sphere (C), which houses the electronics and data recorder. The sphere has a wall thickness of 3.81 cm and external diameter of 71.1 cm. It is made up of two hemispherical forgings bolted on either side of a central ring through which electrical leads are taken. The forgings are manufactured from high-strength aluminium and heat-treated, both in the forged state and after rough machining, to obtain maximum-strength properties with good dimensional stability. The sphere has a working depth of 5,000 m and a theoretical collapse depth of 7,500 m.

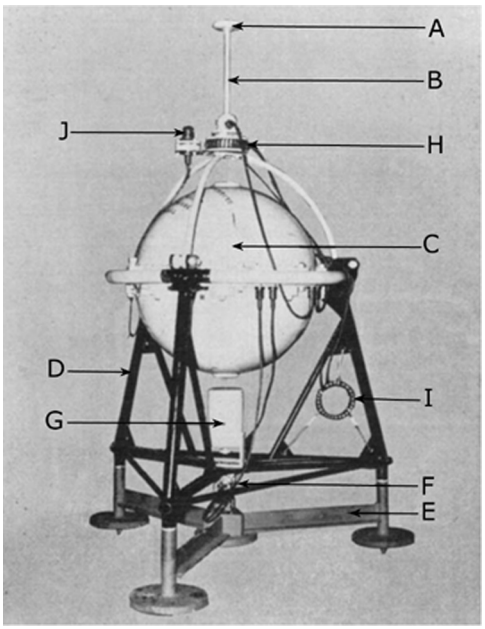

FIGURE 9.8 The assembled EM current meter. (A) Sensing head. (B) Supporting strut. (C) Aluminum sphere that houses the electronics and data recorder. (D) Framework to support the sphere. (E) Triangular base plate used for anchoring the current meter to the seabed. (F) Modified Van-Dorn release to which the base plate is held. (H) Scroll that receives signal from surface for firing the release mechanism. (G) Tilt- and direction-indicating device. (I) Transmission scroll used as a location device. (J) Flashing light used to aid location finding during recovery at night. *(Source: Thorpe et al., 1973.)*

The sphere is supported on a framework (D) and is anchored to the seabed on a triangular base plate (E), to which it is held by a modified Van-Dorn release (F). This release is triggered by a "Pyro" release fired from a 6-V mercury cell. A 10-kHz frequency-modulated signal is transmitted from the surface, received by scroll (H), and fed into a receiver, where the signal is amplified and fed through a discriminator. The signal then passes through a high-Q filter switching a relay and firing a release. Ranges of 4−5 miles are obtainable, and the system demonstrated an operating life of eight months at temperatures down to −4°C. The Pyro release has no explosive force and, on igniting, burns at a temperature of 1,500°C, melting an aluminum tensile rod holding the jaws of the Van-Dorn release. Two Pyro releases are used, the second being triggered via a pre-set clock and acting as a fail-safe device for recovery. On release, the base plate is left on the seafloor and the remainder of the instrument rises to the surface. It has a buoyancy of 14 kg, which gives it an ascent speed of approximately 0.8 m/s, taking 1.75 hours to rise to the surface from a depth of 5,000 m. It floats with about 10 cm of the sphere clear of the water.

The sensing head is 2.1 m above the bottom of the base plate and will be at this height above the seafloor if no sinking occurs. The orientation of the head and the tilt of the instrument on the seafloor have been successfully measured by a simple but effective tilt- and direction-indicating device (G) shown in Figure 9.9. The solid polythene cylinder has a hemispherical upper face marked with 5° rings and radial lines that have a known orientation relative to the electrodes on the sensing head. Above it hangs a compass on a torsionless thread passing through a hollow brass pendulum rod. The solid cylinder can slide within the hollow cylinder, which is shown cut away in Figure 9.9, and is held away from the pendulum against the force of the spring by the magnesium-nickel alloy rod. When the device is in the sea, this rod corrodes and breaks in about two to three hours (some time after the instrument has settled on the seafloor), thereby allowing the spring to force the solid cylinder upward, to trap the compass and pendulum, thus providing a record of the tilt and orientation for examination when the instrument is recovered. The magnet is affected by the base plate and tripod supports, and therefore the direction can only be read to within 4°, but at worst the orientation is known to within 10°, the tilt to 1°, and the direction of tilt to 20°.

A 10-kHz 1-second acoustic pinger with the transmission scroll mounted on the vehicle framework (I in Figure 9.8) is used to accurately time the record-switching sequence and to act as a location device. The instrument, attached to the base plate, is released at the sea surface and allowed to free-fall to the seafloor. A flashing light

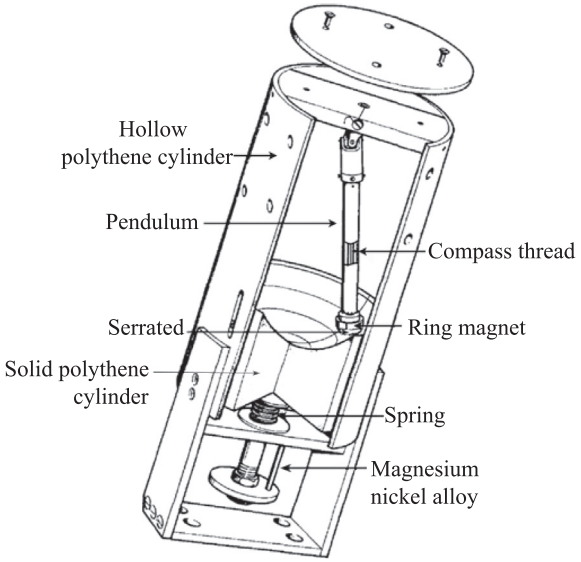

FIGURE 9.9 Tilt and direction indicator. *(Source: Thorpe et al., 1973.)*

(J in Figure 9.8) aids location finding during recovery at night.

A leak detector was housed in the sphere. This consisted of three electrode pairs set in a triangle inside the bottom of the sphere. A short circuit between any of these pairs of electrodes due to the presence of seawater caused a change of 5% in the pinger rate, which would immediately be detectable on a facsimile recorder on board a surface ship.

Current measurements made with this EM current meter in the Gulf of Cadiz revealed rapid and irregular fluctuations characteristic of a highly turbulent flow. Comparisons between records of currents made by the EM current meter and by other meters showed that the EM current meter is a useful instrument for use in the benthic boundary layer.

Head shapes such as the discuss form, developed earlier for use in a ship's log (Tucker et al., 1970) and used successfully also for current measurement in near-rectilinear flows (Thorpe et al., 1973), do not perform adequately in three dimensional flows (Griffiths et al., 1978). In the open-head construction, the magnetic field coil is contained in an epoxy molding of circular or ellipsoidal cross-section so as to minimize disturbance when flow is mainly in the plane of the coil. Four electrodes are mounted within the annulus, and screened electrode leads and coil-drive conductors are led away through the tubular support arms. It has been the practice in sensor heads designed at the Institute of Oceanographic Sciences (IOS) in the United Kingdom to use Monel as the electrode material, although other materials used elsewhere include carbon and silver. Variants of this form of head construction, which was developed at IOS for a vector-averaging current meter (Clayson, 1983), include a 45-cm diameter sensor designed for mounting beneath a surface buoy (Collar et al., 1988); a miniature 4-cm sensor for small-scale resolution; and an experimental sensor incorporating two field coils and pillar-mounted electrodes intended for simultaneous measurement at four levels within 0.5 m of the sea surface. For each of these open forms, extensive tow-tank tests (Griffiths et al., 1978) have shown excellent linearity and off-axis response. For example, the maximum departure from linearity for the 15 cm diameter head is less than ± 2 mm/s in a 1.5 m/s speed range. Perhaps the main relative disadvantages of this form of construction compared with solid heads are the complexity of construction and their fragility, which often requires some form of protective ring or cage to be mounted around the sensor.

Olson's "open" electrode configuration gives rise to vortex shedding from the Helmhotz coils and their supports, thereby adversely affecting the sensor's angular responses. One way of enhancing the sensor's angular response is the choice of a spherical shape to the sensor head. The shape and dimensions of the sensor head are clearly important in the performance of the sensor in a flow field. The flow regime around a solid body depends on the dimensionless Reynolds number, $R_e = \dfrac{VL}{\nu}$, where V is fluid velocity, L is a characteristic dimension, and ν is the kinematic viscosity. Therefore, the design must avoid the critical range of Reynolds numbers if changes in sensitivity and response are not to occur (Griffiths et al., 1978).

Sensor head design affects other aspects of performance. For example, head sensitivity (which is of the order 20 μV/m/s for 1 Watt dissipation) increases as the square root of both the power dissipation in the coil and a characteristic linear dimension of the coil. Head shape rather than size, on the other hand, is generally more important in determining noise level. With the possible laminar flow around streamlined head forms such as the ellipsoid, flow-induced noise is likely to provide the dominant contribution to sensor noise level. Wherever in the spectrum this is true, S/N ratio cannot be improved merely by increasing coil input power. This situation is true in the case of the open sensor. A series of tow-tank measurements (Griffiths et al., 1978) showed that this has associated with it an rms noise level of ~0.6 cm/s at 50 cm/s with a nominal bandwidth of 5 Hz. The thermal noise within the same bandwidth is of order $(1.7 \times 10^{-20} \times RB)^{1/2}$, where B is the bandwidth and R is the electrode source impedance (Collar, 1993). In fresh water, $R \approx 3$ kΩ and in seawater it is ≈ 70 Ω; the corresponding thermal noise that creeps into the current signal is ≈0.07 cm/s and ≈0.01 cm/s, respectively. Noise levels are reduced by taking vector-averaged values over a minute or two, yielding a current resolution typically <1 mm/s.

EM current meters are produced and marketed by several agencies such as Valeport; Cushing Engineering, Inc. (CEI); Marsh-McBirney, Inc. (MMB); InterOcean Systems, Inc.; Applied Microsystems Ltd., and so on.

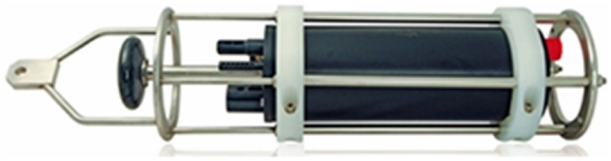

FIGURE 9.10 Valeport-make Midas ECM. *(Source: Valeport brochure, reproduced with kind permission of Kevin Edwards, Sales and Marketing Manager, Valeport Ltd., UK.)*

A Valeport-made Midas Electromagnetic Current Meter (ECM) is shown in Figure 9.10. This small solid-state sensor has been designed specifically for use in open channels where fouling by weed or sewage can be a problem. Valeport's experience in electromagnetic technology has ensured that the Midas is a high-precision instrument that can be relied on to give accurate readings (±0.5% of reading plus zero stability) over a wide flow range (±5 m/s). The control display unit provides a choice of averaging modes, standard deviation of the data, and an optional logging facility. Valeport's latest electronics architecture allows multiple additional sensors and a variety of communications options, making it one of the few multiparameter current meters that allows real-time operation over several thousand meters of cable as well as autonomous deployments. A choice of titanium or acetal housing gives depth rating up to 5,000 m.

Cushing Engineering, Inc. (CEI), employs orthogonal electrodes. This is a concept that has been in use for several years. However, the techniques of application are different. The CEI uses a 7-inch cylindrical flow transducer. Its pressure housing is 64 inches long, with an outside diameter of 7 inches; the total length is 89.5 inches. It weighs 95 pounds in air. This design has a cylindrical flow sensor large enough to house all subsystems. The sensor incorporates an alternating electromagnet and two orthogonal pairs of flow-detection electrodes located near the center of the housing and attached flush with the outside container. Each pair of electrodes senses a voltage proportional to the component of velocity perpendicular to the plane, determined by the axis of the electrode pair and the sensor's longitudinal axis of symmetry. These voltages are conditioned and resolved into east and north components of current by a vector rotator using the output of a flux-gate compass. The current velocity components are then processed into mean values and recorded incrementally on magnetic tape.

Some degree of immunity from the problems caused by changes in flow regime around a solid of revolution can be obtained by mounting the electrodes out from the surface. Furthermore, locating the sensor head away from the sensor's housing will avoid vortex-induced deterioration of the sensor's performance. These two techniques have been adopted in the EM current meters manufactured by Marsh-McBirney, Inc. (MMB), an assessment of which has been made by Aubrey and Trowbridge (1985). Like the CEI current meter, the MMB current meter also uses pairs of orthogonal electrodes mounted along the equatorial plane of its 4-inch spherical transducer. Figure 9.11 shows the MMB current meter (designated Model 585 Adaptive Recording Current Meter). Its pressure housing is 42 inches long, with an outside diameter of 7 inches; the total length is 60 inches. It weighs 95 pounds in air. This sensor has

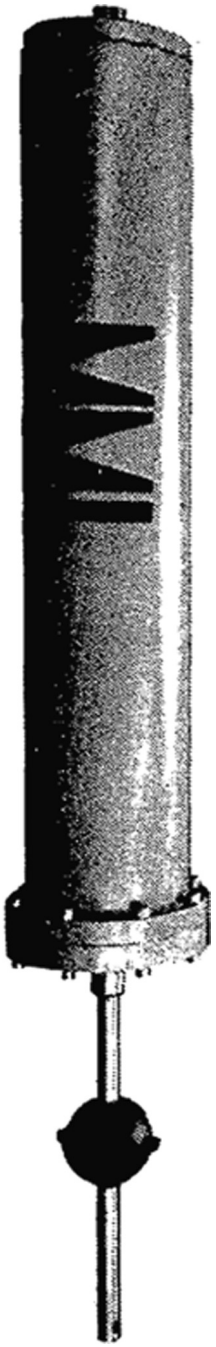

FIGURE 9.11 Marsh-McBirney, Inc. (MMB) current meter, designated Model 585 Adaptive Recording Current Meter. *(Source: Marsh-McBirney, Inc. brochure.)*

a spherical electromagnetic sensor with two orthogonal pairs of flow detection electrodes. A digital geomagnetic compass measures the orientation of the current meter with respect to the magnetic meridian. A microprocessor-based data acquisition system resolves the current vectors into east and north components of currents, computes the mean values of these components, and transfers them to an incremental tape unit for recording.

In current flows near the air-sea interface, where wave orbits are circular in the vertical plane, the vertical cosine response is also important. With poor vertical cosine response, the vertical components of flow can reduce or augment the horizontal component in one horizontal direction either more or less than that in the orthogonal horizontal direction. This can lead to an error in direction of the horizontal component of flow as well as the magnitude. Though a spherical sensor by itself has excellent horizontal and vertical cosine response characteristics, the vertical cosine response of a current meter that incorporated a spherical EM sensor has been reported to have been degraded (Appell, 1979), probably due to current flow distortion as the flow passes over the pressure housing for the electronic circuitries. Performance degradation as a result of current flow masking associated with the electrode housing and the instrument supports indicated the need for refining the instrument's vertical and horizontal angular responses (i.e., tilt and azimuthal responses).

One method of reducing the distortion of the current flow field, generated by the instrument's supports, is the use of advanced designs where the instrument package is mounted within a spherical housing and the electrodes mounted on the equator of this sphere (Lawson et al., 1983). The sphere has proved particularly attractive in that it possesses three-dimensional symmetry and might therefore be expected to exhibit good responses to off-axis flows. However, any sensor head inevitably disturbs the free stream flow and introduces the risk of flow separation. Spherical design has been incorporated into EM current meters commercially manufactured by InterOcean Systems, Inc. (Figure 9.12). Two orthogonal pairs of electrodes and an internal flux gate compass provide the current vector, without the need for a vane. Improved azimuthal response takes better advantage of the inherent dual-axis capability of the sensor. On the other hand, improvement in the tilt response gives rise to a considerable enhancement in the current measurement accuracy when the sensor is used for particle velocity studies in the surface-wave field (Mulcahy, 1978). Ideal cosine-response characteristics are a highly desirable feature when one considers the very high accuracies required to extract mean velocities and, in particular, mean velocity shear in the presence of surface orbital motions. These are the major reasons for the preferential application of the spherical EM current meter for current measurements in the wave zone. As indicated earlier, the InterOcean S4 current meter incorporates the entire instrument within a spherical housing, which can be inserted directly into a mooring line. The resulting instrument dimensions would normally yield critical Reynolds numbers at some point within the working range, but this is forestalled by the use of surface ribs so as to induce a fully turbulent boundary layer throughout the working speed range. Good linearity is thereby achieved.

FIGURE 9.12 InterOcean S4 current meter. *(Source: InterOcean Systems, Inc., brochure.)*

Blanton et al. (2002) reported the application of an InterOcean S4 current meter to study tidal asymmetry in three tidal channels with different morphology (e.g., [1] in a 100-km long coastal plain estuary, [2] a 15-km long tidal creek closed at the end, and [3] a small side-channel of a coastal plain estuary closed at low water) by comparing axial velocity as a function of water level (stage-velocity diagrams). Water current and water depth data were harmonically analyzed for the semidiurnal tide M2 and the over-tides M4 and M6, and the results were displayed in a plot of tidal current versus water level. The effects of the M2, M2 + M4, and M2 + M4 + M6 were compared in order to show how over-tides affect tidal asymmetry in the different systems. Stage-velocity diagrams illustrating the spatial dependence of the relative strength of influence of the over-tides along the axis of the just-mentioned three tidal creeks are shown in Figure 9.13. Progressive addition of M4 and M6 to M2 illustrates how over-tides affect the current velocity asymmetry observed in the different tidal channels. The stage-velocity diagrams for stations along

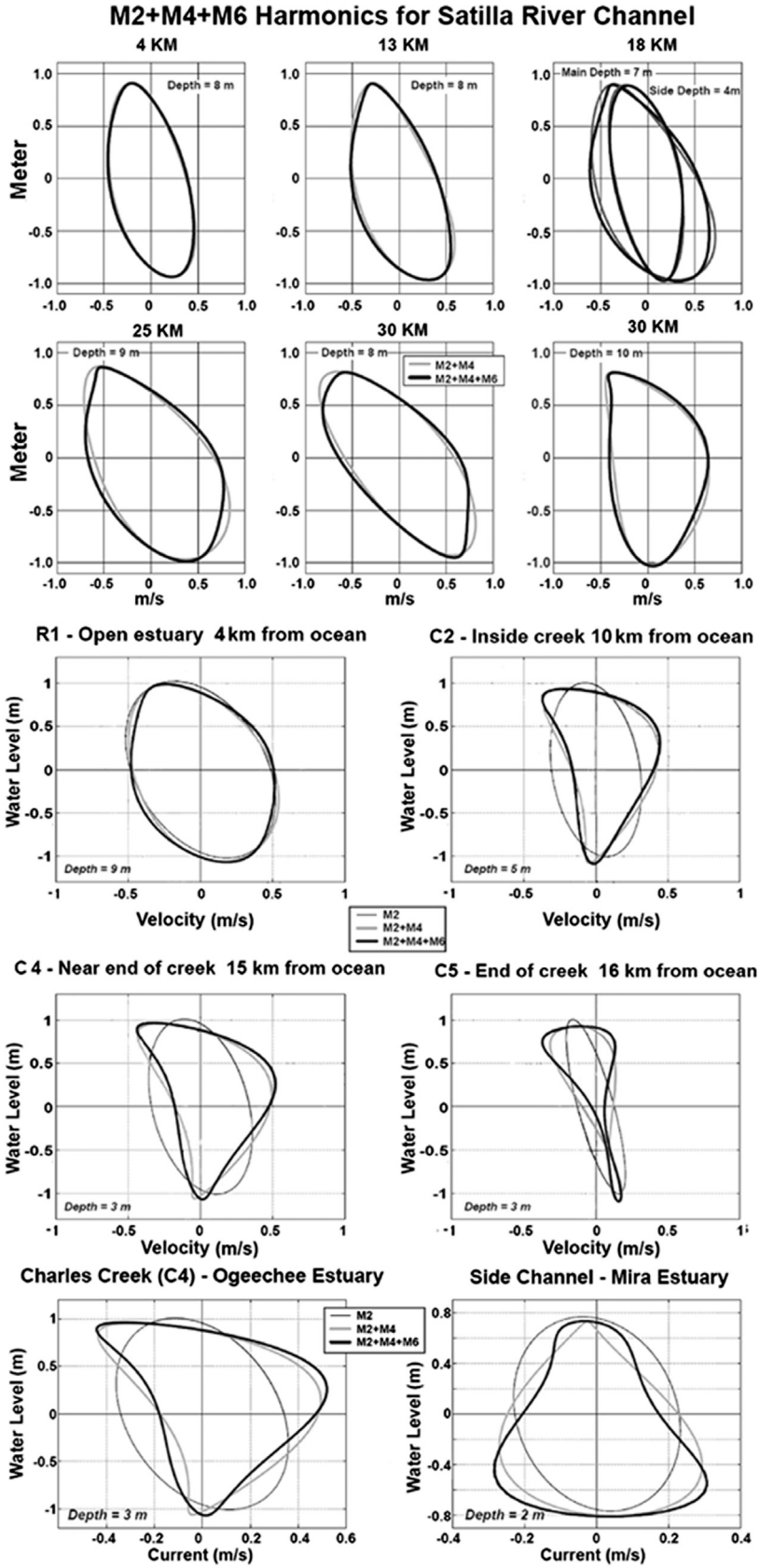

FIGURE 9.13 Temporal progression of water level and tidal current in various estuaries and creeks diagrammatically illustrated in clockwise direction. *(Source: Blanton et al., 2002.)*

the Satilla River show a gradual increase in the strength of the flood and ebb currents. It is seen that the presence of over-tides in the estuary changes the duration of ebb and flood currents. The results show that processes that generate the M4 and M6 over-tides in shallow estuaries and tidal creeks distort the normal sinusoidal character of the tide, as has been recognized by several investigators. The changing relative phase is manifested by the changing orientation of the stage-velocity diagrams, which is related to a steady dissipation of tidal energy along the channel.

For many purposes, power dissipation levels need not exceed a few tens of milliwatts, although at these levels difficulties can sometimes be experienced in calibration in freshwater tanks, where the sensing head source resistance is relatively high and stray potentials are often present in the water as a result of electrical activity in surrounding buildings. In such cases, careful attention to electrical-earthing arrangements is essential but is usually enough to overcome any problems. The mains supply frequency can be intrusive in this respect and is usually evident in the form of an unwanted low-frequency beat at the output of the instrument. For this reason, the choice of head drive frequency should avoid the mains frequency, its harmonics, and its subharmonics; otherwise a spurious DC offset may result in the calibration (Collar, 1993).

Unlike current meters incorporating mechanical sensors, EM current meters have no nonzero velocity threshold. However, response down to zero velocity is of little value unless the output is stable. Potential causes of instability include electrode contamination, biological fouling of the sensor producing a major disturbance of the boundary layer, and changes in the insulation resistance between the magnetic coil and the water. Experience suggests that electrode contamination is generally not a problem in measurement at sea, although care is required when the sensor heads are first put into the flow-tank water for calibration. The water surface in a tow tank frequently carries a thin, almost imperceptible greasy film. The prior addition of a drop or two of detergent to the tow-tank water has been found to eliminate this nuisance. Biological fouling is site and time dependent, but in the open sea it has not generally been found to present any problem.

Instability of the current meter output due to the changes in the insulation resistance between the magnetic coil and the water arises because the coil-water resistance path forms a potential divider with the electrode source resistance, thus permitting a proportion of the coil drive voltage to appear at the output. The need for adequately high ($\geq 10^9$ Ω) coil insulation resistance is particularly acute in the form of construction adopted for the annular head, but with care stabilities to within a few mm/s over periods of several months can be realized.

Overall, electromagnetic sensors potentially possess advantages such as fast response and good linearity, although sensor head design probably represents a more critical area. Interaction of the flow with the sensor head is clearly of fundamental importance. Although much evaluation work has been done in laminar flow conditions, knowledge of response to turbulent conditions is less well developed. This is a difficult area in which to work, partly because turbulence characteristic of the sea is difficult to create in the laboratory tow tank and partly because the EM sensor yields a weighted, volumetric average. Evidence from the few investigations reported in turbulent flow is conflicting, though this may result from the nature of the flow around differing head shapes. Bivins (1975) found up to 20% changes in sensitivity when a cylindrical sensor was subjected to grid-induced turbulence. Results obtained by Aubrey and Trowbridge (1985) using a Marsh McBirney spherical sensor were not conclusive but showed some evidence of a decreased sensitivity. Griffiths (1979), on the other hand, found no evidence for change in experiments using an annular sensor in turbulence created either by a towed cylinder or by a submerged jet.

A disadvantage, perhaps, that can be stated about an EM sensor is that a large magnetic field is required to achieve an adequate S/N ratio for detecting oceanic turbulence (Jones, 1980). This means that it needs a comparatively high electrical power supply to drive the coil. As a compromise, an ingenious technique of conserving coil-drive power in relation to the flow speed has been reported by Desa and Desa (1980). In this technique, a closed-loop circuit enables the coil power of the current meter to be continuously adjusted for current speeds exceeding a preset threshold value. The closed-loop circuit permits less power to be fed to the Helmhotz coils when the electrode potential is large.

In the closed-loop system shown in Figure 9.14, the buffer-amplified output from the electrode-pair is compared with a standard precision voltage reference V_{ref}. The comparator output is used to modify the drive to the coils via the amplitude control stage. The amplitude controller consists of an integrating comparator wherein a DC reference level is compared with the full-wave-rectified output of the oscillator. The output of the integrating

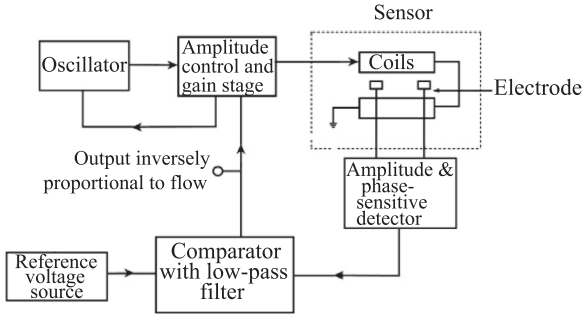

FIGURE 9.14 Block diagram of a closed-loop electromagnetic flow meter system. *(Source: Desa and Desa, 1980.)*

comparator drives the gate of an FET so as to maintain the AC amplitude of oscillation equal to the DC reference level. The integrating comparator output thus alters the coil power so that the difference between the buffer amplifier output and V_{ref} is reduced to a very low level. The closed-loop action thus maintains the electrodes at a constant voltage by altering the coil power when there are changes in water flow velocity.

Because the closed-loop system operates to maintain a constant voltage at the electrodes, Equation 9.1 can be rewritten as (Desa and Desa, 1980):

$$V_{ref} = (V \times B)L \tag{9.3}$$

Because B is directly proportional to the voltage across the coils, V_c, then from Equation 9.3,

$$V \propto \frac{V_{ref}}{V_c} \tag{9.4}$$

The coil voltage will be a maximum at the minimum flow velocity. This minimum is set by the capabilities of the amplification and detection circuitry. In the circuit tested by Desa and Desa (1980), the output of the comparator in Figure 9.14 is limited to a +2 V swing, at which level the output to the coil just begins to clip the rail voltages. At higher water currents than the minimum, the comparator output decreases, thus reducing the coil voltage as outlined. The reference source was equal to 1.600 V with a temperature coefficient of 35 ppm/°C.

Tow-tank results of the flow meter in its open-loop configuration (see Figure 9.5) yielded the sensitivity figures for the current meter. Thus, the coil power and also the sensor output for a known velocity having been determined, it was possible to set the range of flow velocities for the closed-loop system. The sensor output after amplification was approximately 20 mV/(m/s) for a coil power of 2 W. This sensitivity figure was subsequently increased by a factor of 3 for all further measurements.

To set up the closed-loop system for tank calibration in the velocity range 0.12−1.96 m/s, the reference source used for comparison was stepped down to 8 mV, corresponding to 0.12 m/s. The output of the comparator to the amplitude control stage was then equal to about 1.65 V, and this after the gain stage produced an oscillator output of 10 V rms just short of clipping the rail voltages. The upper end of the flow range now automatically adjusts itself to the requisite lower value. Results of calibration of the closed-loop EM current meter in the form of a graph of the reciprocal of the closed-loop output are shown in Figure 9.15. The correlation coefficient was found to be 0.998. The errors observed in this measurement could be largely attributed to the averaging of the closed-loop output, because a filter with a large time constant had to be incorporated into it. The low excitation frequency of 20.8 Hz required a large time constant in the phase-sensitive detector stage to obtain

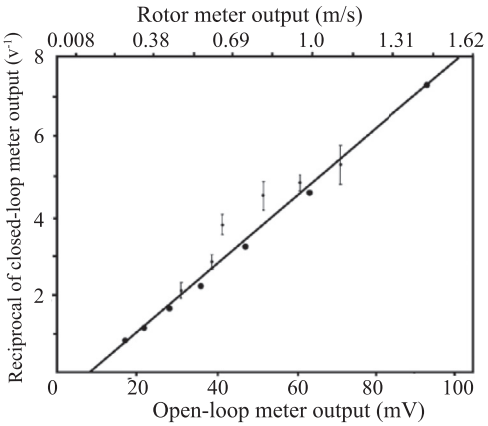

FIGURE 9.15 Reciprocal of the closed-loop EM current meter output with the open-loop meter output in a tank (shown with the best fit through the filled square points) and the corresponding field points (shown with error bars) using a Savonius rotor current meter. *(Source: Desa and Desa, 1980.)*

a low-ripple DC level for error comparison with V_{ref}. This time constant enforced a larger time constant in the comparator to maintain reasonably steady oscillator outputs. The overall time constant was kept equal to several seconds because the type of oceanographic measurements for which the current meter was designed did not demand faster response characteristics.

The location chosen for the field trials of the closed-loop system was an estuary where a large volume of outflow or freshwater to the open sea created layers of differing flow velocities. The reciprocal of the closed-loop output was recorded against the flow velocity as measured by a mechanical rotor current meter with a time averaging of 25 s. The rotor current meter had previously been calibrated in a tow-tank facility and subsequently against the open-loop EM current meter in the field. The field data points and their associated error bars are shown in Figure 9.15 for comparison with the tank calibration points. Data over only a limited range were obtained because these were the prevalent conditions during the field trials. The agreement is surprisingly fair despite the large uncertainty in the rotor current meter measurements brought about by its own inherent limitations and the natural variations of flow normally encountered in the field.

The closed-loop EM current meter feeds more power to the sensor coils when the water-flow velocity is low and less power when the flow signals are large. This type of current meter is therefore useful where long-term monitoring in a high-flow regime is required. In situations where a large range of current velocities is encountered, this system is especially advantageous because power saving of approximately a factor of 1,000 can be achieved for a velocity range of 33 cm/s. Because the S/N ratio is higher at large current speeds, reduced magnetic field as a result of

reduced coil power does not degrade the sensor's ability to detect oceanic turbulence.

The inverse relation between water current velocities and coil voltages is easily converted to read as directly proportional quantities by the use of appropriate inverting circuits. One satisfactorily tested method was to convert the coil voltage to DC and feed it to a function generator integrated circuit chip (a voltage-to-frequency converter). The output frequency of this setup is then directly proportional to the water-flow velocity. This signal is readily transmitted over reasonable cable lengths, as would be required in the case of a submerged flow sensor and an onboard read-out unit.

9.2. ACOUSTIC TRAVEL-TIME DIFFERENCE AND PHASE DIFFERENCE SENSORS

When precise measurement of ocean currents is desired, one seeks linearity, accuracy, stability, freedom from flow disturbance, sensitivity, range, and cosine response (Thwaites and Williams III, 1996). Depending on the application, some features would be more important than others. Unfortunately, hardly any current meter has all the features that are desired. An acoustic travel-time (ATT) difference sensor is not an exception, but it has some admirable qualities, such as linear response through zero velocity, three-dimensional measurements, the ability to measure currents along many axes using one set of circuits, the ability to measure water current flow velocity vectors at a rapid rate over a small volume with little flow obstruction, omnidirectional response, the absence of lower speed threshold, and sensitivity to resolve turbulent fluctuations in the sea. These specialties render ATT current meters valuable for precision current measurements in diverse oceanic environments.

An Eulerian-style current meter incorporating an ATT difference sensor operates based on the principle that the resultant velocity of an acoustic wave propagating in a moving fluid is the vector sum of the fluid velocity and the sound velocity in the fluid at rest. The time required for an acoustic pulse to travel from one transducer to another, or vice versa, is the ratio of the path length to the speed of sound in the fluid. With no fluid flow, the travel-time difference between the transit times of the pulses in opposite directions is zero. When there is a flow, the sound velocity is aided in one direction and retarded in the opposite direction.

In designs where differential travel time is directly measured, two piezoelectric transducers of a given pair are simultaneously excited by voltage steps from 100 to 400 volts at a chosen repetition rate. For every excitation, each of the transducers generates a burst of exponentially damped high-frequency acoustic oscillations (in megahertz range) at the same repetition rate. A mathematical expression relating the current flow speed component (v) along the acoustic path, the acoustic path length (l), the speed of sound in the water at rest (c), and the acoustic pulse travel-time difference (Δt) can be derived as follows: Let the time required for an acoustic pulse to travel from transducer #1 to transducer #2 be T_1. Let us assume that during this travel along the acoustic path length (l), the sound velocity (c) is aided by the current flow speed component (v) along the acoustic path. In this case,

$$T_1 = \frac{l}{(c+v)} \tag{9.5}$$

Let the time required for an acoustic pulse to travel in the opposite direction (i.e., from transducer #2 to transducer #1) be T_2. In this case, the sound velocity (c) is retarded by the current flow speed component (v) along the acoustic path, and therefore T_2 can be expressed as:

$$T_2 = \frac{l}{(c-v)} \tag{9.6}$$

It is obvious that $T_2 > T_1$. Let $T_2 - T_1 = \Delta t$. From Equations 9.5 and 9.6,

$$\Delta t = \frac{2lv}{c^2 - v^2} \tag{9.7}$$

In practice, v is very much smaller than c so that $(c^2 - v^2) \approx c^2$. Based on this approximation, when the transducers stay in the moving fluid, the difference between the up- and downstream sonic travel times (i.e., the travel-time difference, Δt) given by Equation 9.7 is simplified as:

$$\Delta t = \frac{2lv}{c^2} \tag{9.8}$$

From Equation 9.8,

$$v = c^2\left(\frac{\Delta t}{2l}\right) \tag{9.9}$$

As indicated earlier, l is the straight line distance between the transducers of a given pair, v is the mean current flow velocity component along the acoustic path, and c is the sound velocity through the fluid at rest. Equation 9.8 shows that the differential travel time depends on the square of the sound velocity in water. The value of c is known to vary with the water temperature, pressure, and salinity (Urick, 1975). To compensate for variations in c, one method that has been adopted is to determine the mean (T) of the upstream and downstream acoustic travel times and to compute sound velocity using the relation $c = \frac{l}{T}$, thereby adjusting the current flow speed to the correct value (Lowell, 1979). Another method relies on measurements of temperature, salinity, and pressure and application of the

required correction to the assumed sound velocity based on accepted formulae connecting the described three measured parameters. Measurement of current flow components along two orthogonal axes permits computation of the mean flow vector. Inclusion of a magnetic compass provides a magnetic north reference, and the two orthogonal flow components can be rotated into the magnetic components. Use of a third axis orthogonal to both the first and the second axes permits three-dimensional current measurements.

In a self-recording current meter for which the acoustic path length (l) is typically in the range 10−15 cm, it follows from the expression for Δt that the resolution of currents to better than 1 cm/s requires time discrimination to about 10^{-9} s. This emphasizes a need for highly stable, wideband detection of pulse arrivals, which is a critically important factor in achieving a successful design. Aspects of the design and performance of ATT sensors are discussed by Gytre (1976, 1980).

Apart from aspects pertaining to ATT difference discrimination, hydrodynamic considerations are also critically important in achieving the best possible accuracy of current measurements. The principal difficulty that arises in the case of ATT current meters is that of providing rigid mounting arrangements for the transducers, which are typically of order 1 cm in diameter, at each end of an acoustic path of perhaps 10−15 cm without significantly disturbing the free stream flow. Resolution of high-frequency processes requires that any noise contamination in the current meter be significantly reduced. To minimize vortex shedding (i.e., wakes) behind the leading transducers (which modulates the flow velocity field, thereby contributing to errors in the current flow measurements), an acoustic reflector is often used to deviate the ultrasonic beam between the transducers into a V shape (McCullough and Graper, 1979). By thus folding the sound path (see Figure 9.16), most of the travel of the acoustic signal is out of the shadow of the transducer and reduces the effect of turbulence around the sensor probes. In practice, ultrasonic signals are emitted at an angle of 45° to the horizontal plane (when the current meter is deployed with its major axis vertical). The transducers' tips are shaped to make the local currents around them cross the ultrasonic signals at an angle of 90° so that flow signal contamination does not take place. Though the acoustic signal folding technique reduces the primary interference, it introduces wakes from the mirror and its supports. Latterly the development of microprocessor technology has enabled use of redundant paths, so that for a given instrument orientation, the least disturbed paths can be selected in subsequent processing.

The basic ATT technique has been implemented in various forms for a range of applications. Examples of commercially available *in situ* recording ATT current meters in common use are the Simrad Ultrasonic Current Meter (UCM), manufactured by EG&G Inc.; the Acoustic Current Meter (ACM), manufactured by Neil Brown Instrument System (NBIS); and the one manufactured by Falmouth Scientific, Inc. These current meters are excellent instruments, but, like many other current meters, they are likely to be limited by their horizontal response characteristics. Saunders (1980) investigated the errors due to noncosine response in the horizontal plane (i.e., azimuthal response) in the case of the NBIS ACM. According to the manufacturer's specifications, the overall accuracy of the vector magnitude of the current is ±0.5 cm/s or 3%, whichever is greater. The direction accuracy is specified as ±5° for currents greater than 10 cm/s. At a current speed of 50 cm/s, the vector magnitude should be accurate to about ±1.5 cm/s. The manufacturer specifies horizontal cosine response error of ±2% of the vector magnitude over a 360° rotation.

Deviation from the ideal azimuthal response usually arises due to the presence of the support rods surrounding the sensor. For example, deviation as great as 5% in

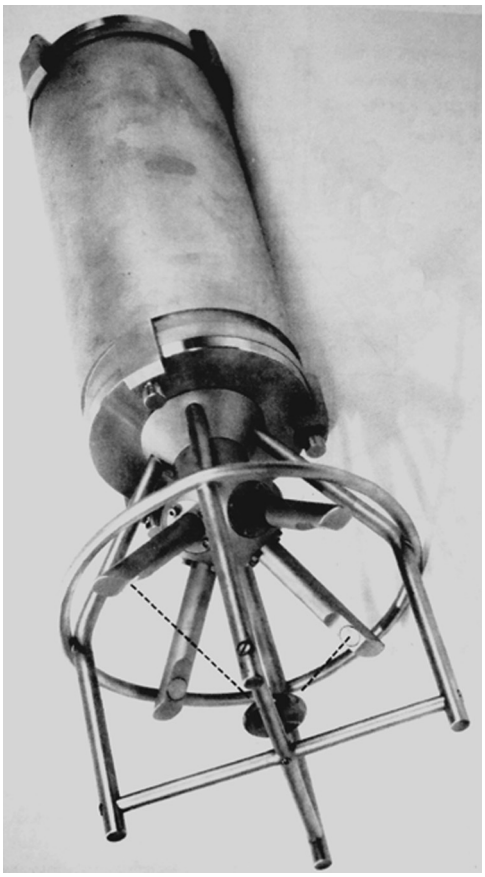

FIGURE 9.16 ATT current meter (original Christian Michelsen Institute design). Hatched line shows one of the two orthogonal acoustic paths via a reflector. *(Source: Collar, 1993, reproduced with kind permission from National Oceanography Centre, Southampton SO14 3ZH, United Kingdom.)*

magnitude due to the presence of support rods has been reported in the case of VACM (Woodward and Appell, 1973). The NBIS ACM also has four support rods; therefore, investigation of a possible departure from a "cosine response" due to the support rods in the case of NBIS ACM is justified. This source was confirmed by tests of the horizontal response of an earlier model of the NBIS ACM by Appell (1978) and McCullough and Graper (1979). Tow-tank tests were carried out at David Taylor Naval Ship Research and Development Center (DTNSRDC) at an angular increment of 15° in the horizontal plane at tow speeds of 12.7 cm/s (nominal) and 31.1 cm/s (nominal) and at the National Space Technology Laboratories at an angular increment of 2° in the horizontal plane at tow speed of 10 cm/s. The direct voltage outputs from both axes of the current meter were fed to digital voltmeters operating on an IEEE-488 data bus. The tow carriage speed values and the ACM voltages were averaged over 1-minute intervals.

Because the carriage speed could not be held exactly constant, the output of each axis was normalized by the carriage speed. This quantity is designated as the *gain* of each axis. The unit of the gain is mV/(cm/s). The nominal gain for NBIS ACM is about 7 mV/(cm/s). In general, this value may vary slightly with the axis under consideration and the orientation of the current meter housing. Modification of the wake structure behind the support rods and the transducer supports may also render the gain a weak function of speed.

The theoretical gain curves assuming a maximum gain of 7 mV/ (cm/s) are plotted for comparison. Certain deviations from the theoretical cosine and sine curves are apparent, but in general, the observed points seem to fit the theoretical curves rather well.

The relative gain amplitude error $\varepsilon(\theta)$ is defined by (Saunders, 1980):

$$\varepsilon(\theta) = \frac{(G_x^2(\theta) + G_y^2(\theta))^{1/2} - \bar{G}}{\bar{G}} \tag{9.10}$$

where $G_x(\theta)$ and $G_y(\theta)$ are the gains at the orientation, θ, of the current meter case (i.e., current meter housing) and

$$\bar{G} = \frac{1}{N}\sum_{i=1}^{N}\left\{G_x^2\left(\theta_i\right) + G_y^2\left(\theta_i\right)\right\}^{1/2} \tag{9.11}$$

Here θ_i, $i = 1, \ldots..., N$ are all the case orientations for which the gains are measured. The direction error (ϕ) is defined as:

$$\phi(\theta) = \theta - \tan^{-1}\left(\frac{G_y(\theta)}{G_x(\theta)}\right) \tag{9.12}$$

The relative gain amplitude error is a measure of fractional error in speed when the current meter case is oriented at an angle θ, whereas the direction error is the error in direction that will be made when the case is oriented at angle θ. These parameters will approximate the error when it is assumed that the case is oriented at the angle defined by $\tan^{-1}\left(\frac{G_y}{G_x}\right)$, providing $|(\phi)| \ll 1$. It should be noted that ε achieves local maxima at odd multiples of 45° and minima near the multiples of 90°. The maximum deviations of ε are of the order of $\pm 6-8\%$, whereas the maximum direction errors are of the order of $\pm 5°$.

Depending on the direction of current flow, the wakes from the tension rods can interfere differently with the acoustic sampling volume, thus deteriorating the cosine response of the current meter. When the current meter is rotated 45°, the wake from the support rod directly crosses the acoustic sensing volume, thus indicating a speed deficit. The role played by the wakes shed by the tie rod is distortion of the theoretical cosine response. As expected, the largest contribution is the "cosine" response of the first harmonic. It is seen that at $\theta = 0°$, the third harmonic contribution is positive (enhanced observed speed). By the time $\theta = 30°$, there is no contribution, because the effects of the wake deficit and streamline compression cancel one another. From 30° to 90°, the wake effect dominates, thereby producing the speed deficit. The same description applies to the other quadrants. Another expected effect is due to the wakes of the transponder support struts.

It appears that if the orientation of the current meter housing (case) relative to the current is known throughout the sampling period, it may be possible to correct for the imperfect horizontal response of the current meter. Because the case orientation is obtained only once every eight samples, the described requirement necessitates that the case orientation and the current direction both be slowly varying functions of time with respect to an 8-minute time scale. In general, however, this situation will not probably exist except for mooring in rather weak flows far from surface. The orientation is not a slowly varying function of time with respect to the sampling interval. However, it is conceivable that sufficiently smooth conditions may be more common.

Based on evaluation tests on four NBIS ACM current meters, Saunders (1980) found that if a calibration is to be used to correct for case orientation effects, a separate calibration must be used for each current meter. His studies gave an indication that the horizontal response may be speed-dependent as well as instrument-dependent. It was also inferred that the major source of error in horizontal current measurements utilizing the NBIS ATT current meter is due to its imperfect horizontal response. If the torsional motion of the current meter is absent or varies slowly enough, the amplitude error due to the horizontal response could be reduced by about a factor of 5 and the directional error reduced by a factor of 2.

Trivett et al. (1991) and Thwaites and Williams III (1996) conducted extensive studies of ATT current meters, and according to them the error sources for an ATT current meter include:

- Time-average flow obstruction from wakes
- Time-varying disturbances from wakes, vortex shedding
- Potential flow disturbance
- Zero offset bias
- Electronic nonlinearity
- Electronic noise

Electronic nonlinearity is described by Williams III (1995). Vortex shedding from bluff structural members is a significant contributor to measured velocity noise. The dominant frequency of vortex shedding for cylinders is given by the expression (Blevins, 1977):

$$F_s = \frac{0.2v}{d} \tag{9.13}$$

Here F_s is the frequency in Hertz, v is the fluid velocity relative to the cylinder, and d is the cylinder diameter. ATT measurement of flow velocity can be thought of as measuring a line integral of velocity along the acoustic path. If the acoustic path is downstream and at an angle to the cylinder, the measured flow noise will scale with:

$$\text{Velocity noise } \alpha \frac{vd}{L} \tag{9.14}$$

In this equation, L is the acoustic path length. If the structure upstream of an acoustic path is streamlined but stalled, its wake will also form a vortex street (Abernathy and Kronauer, 1962). To reduce the measured flow noise associated with vortex streets caused by the sensor, the ratio of cylinder diameter to acoustic path length needs to be minimized. The path length cannot be made large and still measure small-scale turbulence. To avoid Strouhal resonance, it is desirable to minimize the cross-sectional thickness of the sensor structure that supports the acoustic transducers consistent with structural considerations of strength and stiffness.

Falmouth Scientific, Inc. (FSI), reported a different configuration of the acoustic current meter—acoustic phase shift current meter (Figure 9.17). The current measurement technique FSI used was invented by Brown (1992) at Woods Hole Oceanographic Institution. The theory of operation of an acoustic phase shift current meter is as follows (Brown, 1992): If we consider an acoustic path with two transducers at points A and B where each transducer is alternately transmitting and receiving, the total phase shift between the received and transmitted acoustic signals is as follows.

$$\Theta_{ab} = \Theta_{ta} + \Theta_{rb} + \Theta_{ttab} + \Theta_{rec} \tag{9.15}$$

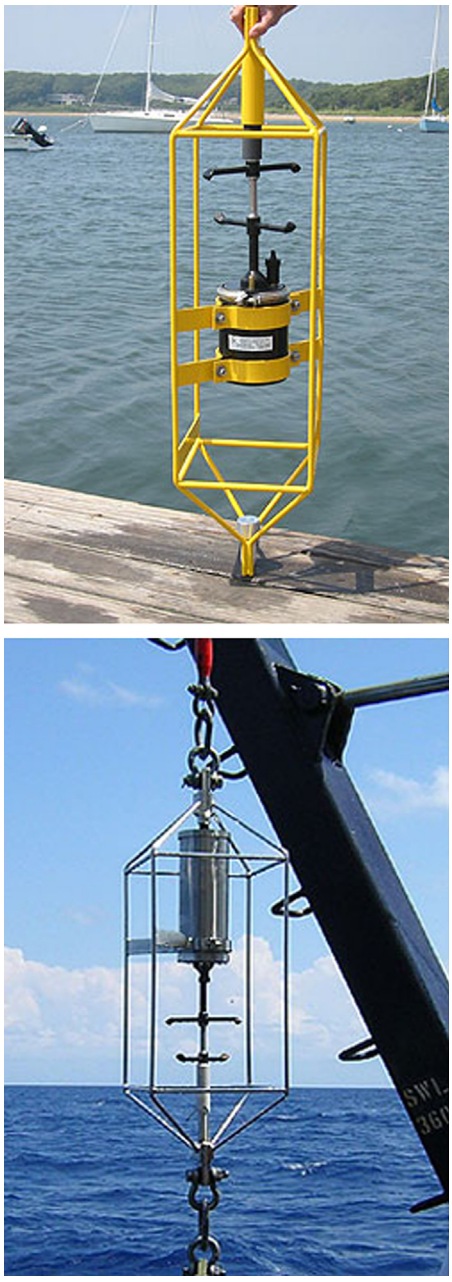

FIGURE 9.17 Falmouth Scientific, Inc. 3-D Acoustic Current Meter, incorporating acoustic phase-shift measurement principle, in protective frame. *(Courtesy of Falmouth Scientific Inc.; www.falmouth.com/sensors/currentmeters.html.)*

$$\Theta_{ba} = \Theta_{tb} + \Theta_{ra} + \Theta_{ttba} + \Theta_{rec} \tag{9.16}$$

In these expressions, Θ_{ta} and Θ_{tb} are the phase angles between the applied voltage and the resulting acoustic pressure wave for transducers A and B acting as transmitters. Similarly, Θ_{ra} and Θ_{rb} are the phase angles between the output voltage and the arriving acoustic pressure wave for transducers A and B acting as receivers.

Θ_{ttba} and Θ_{ttab} are the phase shifts due to the acoustic travel times from $A \rightarrow B$ and from $B \rightarrow A$, respectively. Θ_{rec} is the phase shift through the receiver. For any piezoelectric transducer driven by an essentially zero impedance generator or loaded by an essentially zero impedance receiver, the transmitting and receiving phase angles between the electrical current and the acoustic pressure wave are identical. Therefore, $\Theta_{ta} = \Theta_{ra}$ and $\Theta_{tb} = \Theta_{rb}$. Substituting these in Equations 9.15 and 9.16, and subtracting Equation 9.16 from Equation 9.15 yields:

$$\Theta_{ab} - \Theta_{ba} = \Theta_{ttab} - \Theta_{ttba} \tag{9.17}$$

As the acoustic waves travel from one transducer to the other along the acoustic path length l, the sound speed c in the flow medium is aided or retarded by the current flow speed component v along the acoustic path, depending on the direction of v relative to that of the acoustic wave propagation. Thus, as indicated in Equations 9.5 and 9.6, the time T required for an acoustic wave to travel from one transducer to the other and vice versa along the acoustic path length l differs as a function of the water flow velocity component along the acoustic path. This difference in travel times of the received acoustic signals introduces corresponding phase shifts, given by $\Theta_{ttab} = \dfrac{\omega l}{c - v}$ and $\Theta_{ttba} = \dfrac{\omega l}{c + v}$, where ω is the angular frequency (radian/s) of the acoustic wave and v is the water flow velocity (cm/s) component along path $A \rightarrow B$. Thus, Equation 9.17 can be modified as:

$$\Theta_{ab} - \Theta_{ba} = \frac{\omega l}{c - v} - \frac{\omega l}{c + v} = \frac{2\omega l v}{c^2 - v^2} \tag{9.18}$$

In Equation 9.18, $(c^2 - v^2) \approx c^2$, so that,

$$\Theta_{ab} - \Theta_{ba} = \frac{2\omega l v}{c^2} \tag{9.19}$$

From Equation 9.19,

$$v = c^2 \left(\frac{\Theta_{ab} - \Theta_{ba}}{2\omega l} \right) \tag{9.20}$$

Use of the acoustic phase shift principle eliminates the need for very high speed circuits by heterodyning the two received high frequency carrier signals to obtain a significantly smaller difference frequency (i.e., *beat frequency*) and by measuring the phase difference at the beat frequency with low power circuits.

The FSI acoustic phase shift current meter has four "fingers". Each finger houses two acoustic transceivers. The transceivers are used to create four acoustic paths. The flow velocity is measured by comparing phase shifts of sound pulses traveling along three of the four acoustic paths. One path, which is contaminated by the wake from the center support strut, is always disregarded.

To be able to deploy the instrument for several months using battery power only, the power consumption of the instrument needs to be very low (on the order of 10 mA). For this, first the measurement technique uses direct acoustic paths and not reflected sound (for example, from a mirror). This reduces the power dissipated into the water and thus the power required to operate the instrument. Second, the instrument measures phase shifts of the acoustic signals along the paths, not the time of travel along the individual paths. The advantage of measuring phase shift is that it can be accomplished with slower circuits than measuring the time of travel. Slower circuits in turn require less power to operate. The accuracy claimed for current measurement using this device is $\pm 2\%$ of reading or ± 1 cm/s. The dynamic range is ± 600 cm/s. The accuracy of the directional measurement is specified as $\pm 2^\circ$ (Kun and Fougere, 1999). The instrument is protected from mechanical damage by its protective frame. The frame can also be used to tie the instrument to a mooring cable.

In near-bed benthic boundary layer studies, Reynolds stress is an important parameter. Correlation of fluctuations in velocity components in a boundary layer flow represents turbulent exchange of momentum across streamlines. Averaged over many burst and sweep events, the correlation of velocity fluctuations normal to the boundary with streamwise velocity fluctuations is Reynolds stress (Williams III and Beckford, 1999). Exchange of fluid is the dominant stress-carrying process from the viscous sublayer to the outer boundary layer. In this region, millimeters to meters, the stress is constant, and a single measurement of Reynolds stress represents the shear stress at the boundary. Sediment transport and boundary layer mixing require estimates of the bottom shear stress. Reynolds stress measured within the inertial sublayer represents the boundary layer shear stress because within this region, stress is carried by turbulent exchange of momentum. In stationary, homogeneous flow, the stress in this region is constant, so a measurement at one height represents the stress at the boundary, even if the boundary is rough. If a current meter can measure this turbulent exchange of momentum, it will be a useful tool for boundary layer research.

With a view to achieving improved performance to meet the needs of near-bed benthic boundary layer studies, Williams III (1985) designed a novel ATT current meter known as a *Benthic Acoustic Stress Sensor* (BASS). BASS uses a braced metal frame of small-diameter rods to minimize flow noise, but this requires external electrical cables that are thicker than the structure cage rods. The BASS sensor has no undisturbed flow directions, but all horizontal flow directions are pretty good (Thwaites and Williams III, 1996).

BASS is a pulse travel-time acoustic current meter with four axes arranged about a 15-cm diameter measurement

volume. It measures current flow velocity vectors with an accuracy of 0.3 cm/s and precision of 0.03 cm/s and can sample the flow speed at a 5 Hz rate. An assembly of sensors in a vertical array permits profiles of mean velocity, turbulent kinetic energy, and Reynolds stress to be obtained. BASS arrays have been deployed to depths of 4,800 m on instrumented tripods to estimate bottom stress and to monitor the inner boundary layer. The omnidirectional response, absence of velocity threshold, nonobstructive design, and high resolution of BASS renders it ideal for measurements in locations where current flow speed ranges from 0.5 to 70 cm/s and direction varies through all horizontal angles.

The important design criteria for BASS were that it measure water current flow velocity vectors at a rapid rate over a small volume with little flow obstruction, be omnidirectional in response, have no lower speed threshold, and be sensitive enough to resolve turbulent fluctuations. In addition, the constraints of field deployments required it to have low power consumption, be durable, and have redundancy to recover a vector if an axis were disturbed. The BASS system achieves these goals by using small transducers to measure flow speeds via unobtrusive acoustic pulse travel-time measurements. Four pairs of transducers surround a 15-cm-diameter water volume to measure speed along four axes, thus giving a complete velocity vector with an additional redundant axis. The sampling rate can be set as high as 5 Hz and the power consumption is low enough.

As shown in Figure 9.18, the acoustic transducers in the sensor are carried on two vertically separated rings. Each axis is inclined 45° to the planes of the two rings and spaced 90° in azimuth. BASS uses a lead titanate–zirconate piezoceramic transducer that is 9.5 mm in diameter, 1.27 mm thick, and resonant at 1.75 MHz. The central lobe of the acoustic beam is about 6° wide, giving a spot size of 15 mm at the location of the opposite transducer. This requires alignment within 2°. This may not be the optimum size. According to Williams III et al. (1987), a 5-mm-diameter transducer would be more tolerant of alignment errors and have lower flow disturbance than the existing one and might still have enough gain for a good S/N ratio over a 150-mm path. However, the 9.5-mm transducer is a reasonable compromise for gain, flow disturbance, and alignment sensitivity as well as manufacturability and cost.

As Figure 9.19 shows, the transducer is cast in a rigid urethane (Conap DP-10767) and faced with a soft urethane matching the acoustic index of water (Conap EN-4). It is exposed to hydrostatic pressure and transmits a pressure wave equally from both faces when electrically driven. The mold accurately aligns the transducer with its faces elevated 45° from the mounting flange and aligned with its center 2.3 mm from the inner corner of the rectangular cross-section support ring. Because a burst of many cycles is transmitted and reflections from the early part of the burst transmitted from the back face could add to the later portion of the burst transmitted from the front face, it is important to minimize the amplitude of the reflections along the acoustic axis. The avoidance of any surface parallel to the transducer in the back does this, and the scattering from edges is too diffuse to contribute a measurable effect at the opposite transducer. Little refraction or reflection occurs at the EN-4 facing, and because this is slightly convex, what

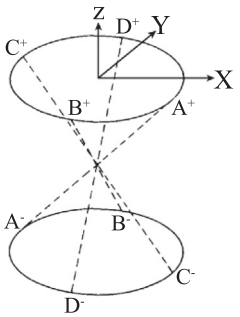

FIGURE 9.18 BASS sensor geometry. Four acoustic transducers (each 1 cm in diameter) are spaced 90° apart in azimuth at the locations indicated by the letters on each of the upper and lower 10-cm diameter rings. Under typical deployment geometry, the measurement path is inclined 45° to the horizontal. The wakes of the support rings and of the transducers lie outside the measurement volume for near-horizontal flows. *(Source: Williams III, 1985.)*

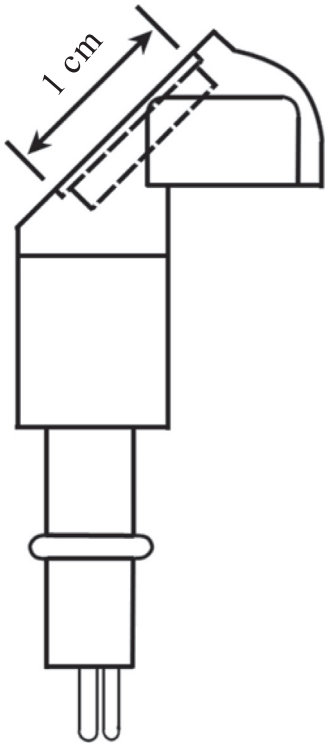

FIGURE 9.19 BASS sensor. *(Source: Williams III et al., 1987; ©American Meteorological Society. Reprinted with permission.)*

reflection does occur is defocused and thus attenuated at the opposite transducer. The transducer is connected through an integrally molded connector to urethane-jacketed RG-316 coaxial cable and then to the electronics pressure housing end cap.

Because of the particular geometry used in BASS, flow disturbance to the measurement volume is minimal for near-horizontal flows. The sensor is linear in flow velocity along any axis up to 120 cm/s and free of wake effects. Deviation from cosine response is less than 5% of the flow speed for all horizontal flows, and for flows out of the horizontal plane it is within 20° of an acoustic axis. This is possible because the transducers are small ($\sim$1 cm^3) and their supporting structures are thin (0.3 cm diameter). Thus, the wake of the structure is not great, and what wake there is crosses the measurement path only for a small percentage of its length. The major flow obstruction is the supporting ring for the sensor cage. This does not shed a wake into the measurement volume until the flow is tipped to about 50° from horizontal. If an individual axis lies within 20° of the flow (mean stream more than 25° out of the horizontal), the wake of one transducer influences the velocity along that axis significantly, and that axis cannot be used for the vector velocity determination. Fortunately, only one such disruption can occur at a time. System redundancy leaves three axes, which can provide all the information needed to measure the velocity vector.

Differential travel-time measurements can be made with pulses of acoustic energy, in which case time differences are measured, or with continuous waves (cw), in which case phase differences are measured. The former method is selected in BASS (a pulse consisting of 16 cycles at 1.75 MHz is transmitted from both transducers of a selected path driven in parallel) because, although it requires more power, it permits simple multiplexing so that many axes can be measured with one set of circuits and each axis can be measured with the transducers connected normally and reversed. The measurement of a single-flow component requires a little over 200 μs, which is the travel time for pulses crossing the measurement volume with the transducers connected normally and again with the transducers connected in reverse. By electrically reversing the transducers, offsets in the electronics can be subtracted. Doing this reduces the noise and drift of the measurements.

Williams III (1985) has provided a detailed description, with schematic illustration, of how precision measurements are accomplished in BASS. Deviations of 0.3 cm/s between sensors can result due to capacitance differences of different sets of transducers and cables. This offset limits the absolute accuracy of the velocity measurement to 10 times the pulse-to-pulse variation, but because the offset is fixed for each deployment of the system, it does not affect the turbulent quantities measured. To avoid aliasing (i.e., leakage of high-frequency energy present in the signal into a lower-frequency portion of the spectrum), the signal must be sampled at twice the maximum frequency present. The 15-cm diameter of the BASS sensor requires a sample rate of 1.6 Hz for a maximum water current speed of 25 cm/s, and a 2-Hz sampling rate is generally used. A sample volume of 15 cm diameter and a sampling rate of 2 Hz capture the turbulent scales of interest.

Good performance is achieved by minimizing the sensitivity of the system to the large and the variable capacitance of the long transducer cables and by isolating each timing circuit from the disturbances created by the other when a pulse is detected. These are described electronically as lowering the impedance of the first electronic stage, the multiplexer, and minimizing crosstalk. Electronic drifts are removed by reversing the connections to the transducers. Finally, the time differences between the first pulse arrival and the second pulse arrival are measured and digitized.

According to Williams III (1985), the horizontal and vertical cosine response, as determined from tow-tank test results, is close to ideal, with a maximum error of 5% of the speed along either axis until the vertical angle causes the flow to come within 20° of an acoustic axis. With regard to the sensitivity of the sensor to oscillatory flows, it was found that there is hardly any change in sensitivity or "zero offset" due to oscillations from less than a sensor diameter to several times the diameter.

Because the sensors are cable-connected to the electronics housing with 6-m-long cables, a tower of sensors and spacer cages can be constructed to obtain vertical distributions of mean and turbulent velocities. The tower must be rigid and fixed; to achieve this structure it is supported within a bottom tripod, as illustrated in Figure 9.20. The flow disturbance of the tower is not significantly different from that of a sensor cage (see Figure 9.21), and this prediction has been found to be true based on tow-tank test results. The tripod would add significant flow disturbance only near the legs, which are sufficiently away from the tower except for the topmost sensor. No large structures such as electronics housings or buoyancy modules are at the same height as a sensor. Also, the sensors are at least 2.5 buoyancy spheres and pressure-cylinder diameters away in the vertical.

With the bottom tripod illustrated in Figure 9.20, water-flow velocity measurements can be made to within 30 cm of the seabed. The ability to measure Reynolds stress means that no dependence on logarithmic velocity profiles is required to estimate the total stress above 30 cm. For a wide range of current speeds, BASS can measure turbulent scales extending into the inertial subrange. The instrument mounted on a deep-sea tripod provides the inner boundary layer measurements required to describe the benthic boundary layer dynamics.

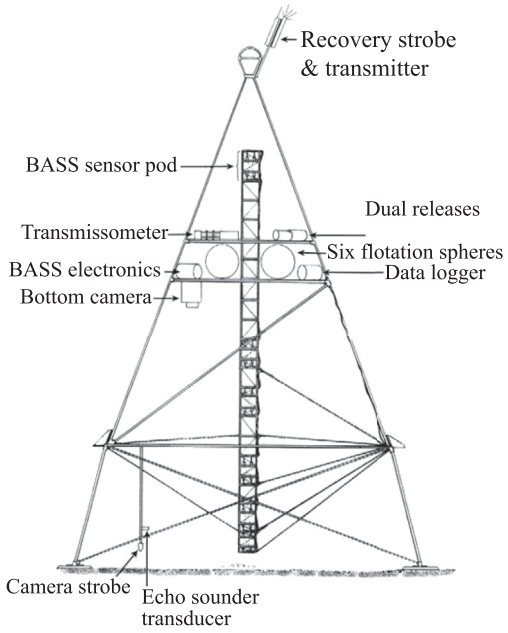

FIGURE 9.20 BASS tripod and sensor tower. The tower at the center of the tripod contains velocity sensors at 0.25, 0.5, 1, 2, 2.5, and 5 m. The instrument housings, buoyancy, and transmissometer are concentrated at 4 m. The lower frame is jettisoned for instrument recovery. *(Source: Williams III, 1985.)*

For deep-water measurements, the heavy lower portion of the tripod is jettisoned by acoustic command when recovery is desired. The upper portion carrying the tower and electronics floats to the surface, and the rising tower assembly is tracked acoustically for pickup. In shallow water, a somewhat different tripod system is used, which is recovered using an acoustically released float and recovery cable. BASS has been very successful at measuring currents, shear, and Reynolds stress (the turbulent transport of momentum).

In ATT current sensing, the "zero point" is not inherent to the sensor and therefore must be determined by calibration in still fluid. This is an important but troublesome chore in the cable-connected sensors of BASS in which flexure of the cables, when dressed on the BASS tripod, changes their capacitance (Williams III et al., 1987). In BASS, after the tower of two to seven sensors is assembled, the urethane-jacketed coaxial cables are tie-wrapped to wire guys and the legs of the tripod. Only then can the zeros be measured. These values are determined by casting the sensors in carrageenan gel or by bagging them in plastic film and deploying the tripod while measuring the flow inside the bags (Morrison et al., 1993).

Decomposition of current velocity fluctuations into vertical and horizontal components has been effective since the first BASS deployments. Sensitivity, linearity, and freedom from flow disturbance have allowed BASS to measure Reynolds stress. Figure 9.22 shows a short segment of an event record from a 1984 deployment at the HEBBLE site (Grant et al., 1985). Following the success of BASS, Thwaites and Williams III (1996) started developing its derivative, known as Modular Acoustic Velocity Sensor (MAVS), to achieve better performance by removing some of the obstacles found in the BASS. MAVS is also a three-axis ATT current meter that measures differential-acoustic travel time in a small measurement volume (see the photograph of a MAVS sensor in

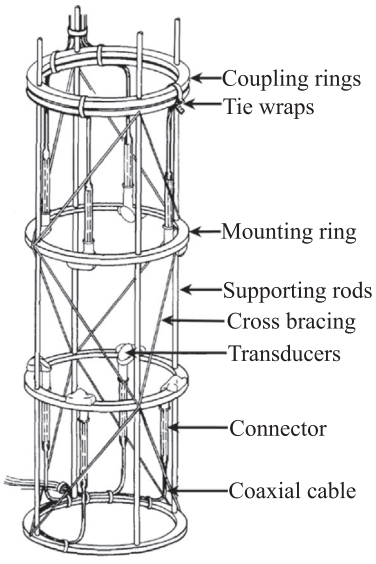

FIGURE 9.21 Sensor cage of BASS. *(Source: Williams III et al., 1987; ©American Meteorological Society. Reprinted with permission.)*

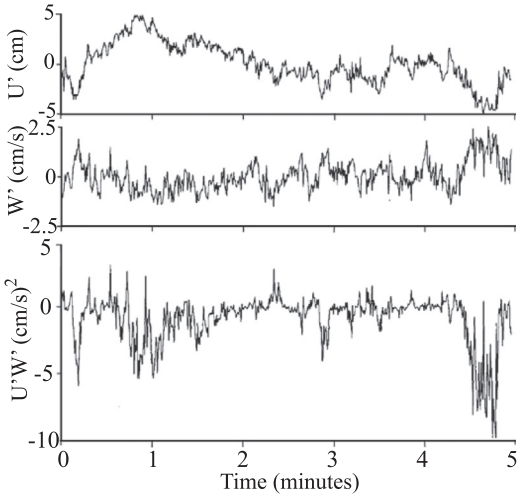

FIGURE 9.22 BASS data. The horizontal velocity fluctuations in the top plot, when multiplied by the vertical velocity fluctuations in the middle plot, give the bottom plot. The average value of the correlation weighted by the density of the fluid is the Reynolds stress. Reynolds stress is an average of this bottom plot, but structure in the flow is revealed by the predominant negative correlation in sweeps and ejections. *(Source: Williams III et al., 1987; ©American Meteorological Society. Reprinted with permission.)*

Chapter 2). Each acoustic axis on MAVS is oblique, with the axes 45° to the plane of the rings and passing from one ring to the other. The paths are spaced 90° in azimuth around the rings, one path going obliquely up, the next obliquely down, the third obliquely up, and the fourth obliquely down. Opposite paths—1 and 3, for example—when subtracted give one horizontal component of flow and when added give the vertical component of flow. The other opposite paths, 2 and 4, when subtracted give the other horizontal component of flow and when added give a second realization of the vertical component of flow. Because the vertical components are the same, if one axis fails for some reason, the full vector flow can be reconstructed using the redundant vertical components. In the normal rotation into Earth coordinates (or into instrument coordinates), all axes are used for each Cartesian component. *U, V,* and *W* components are estimated as follows (as per Dr. Albert J. Williams III, Woods Hole Oceanographic Institution, personal communication):

$$U = (-V_a + V_b + V_c - V_d) \times \beta \tag{9.21}$$

$$V = (-V_a - V_b + V_c + V_d) \times \beta \tag{9.22}$$

$$W = \frac{(V_a + V_b + V_c + V_d) \times \beta}{\sqrt{2}} \tag{9.23}$$

In these equations, β is the scaling factor. Thus, MAVS measures the instantaneous flow velocity vector along four acoustic paths resolved into Cartesian Earth coordinates and thus the 3-D vector velocity in a cylindrical volume 10 cm in diameter and 9.5 cm high. This small region can be assumed to be uniform in velocity for purposes of resolving Reynolds stress down to a scale of 20 cm, although there are certainly turbulent fluctuations down to the dissipation scale of millimeters that are not resolved by the 10-cm acoustic paths in MAVS. Such a measurement is valuable for studies of sediment transport in which the shear stress on the bottom is the forcing function for erosion and a barrier to deposition. It may be noted that the energy content of the fluctuations is less at the 1-cm scale than at the 10-cm scale of the sensor if the boundary that generates the Reynolds stress is several sensor diameters away. The goal of developing MAVS was to give oceanographers access to the ATT technology in an affordable and easy-to-use form. The sensor was designed to reduce the amount of labor required in its manufacture compared to a BASS sensor, together with achieving reduction of flow disturbance error when flows are steeper than 30° from the horizontal. Other attributes of MAVS are low cost, small size, higher accuracy, good cosine response to current direction (immunity to off axis flow and gain independent of attitude), lack of bias in a wave environment, ability to measure turbulence and the Reynolds stress, resistance to fouling (helped by no moving parts), ability to measure near a boundary, and enhanced accuracy at low current speeds (linear response through zero flow). In MAVS, the horizontal cosine response is excellent due to symmetry, and the vertical cosine response has been improved by fairing the rings that support the transducers. If the cost and size of the sensor can be kept small enough, arrays of current sensors could be deployed to measure flow fields, not just the time series of current at one or two points. Measurement and understanding of organized structures, such as Langmuir cells, could benefit greatly from such an array.

Whereas a BASS sensor requires a great deal of labor to build, thereby making it expensive, the MAVS sensor requires fewer labor-intensive potting steps of molding the transducers and cables in polyurethane. MAVS is only a single-velocity sensor that outputs a serial datastream to a user-supplied logger. It has been noted that one of the limitations of BASS is that cable flexing alters the "zero offset" of the velocity measurements by slightly changing the cable capacitance (Morrison et al., 1993). When the cables are flexed or retied, the zero offset typically changes by one-third to one-half cm/s. Based on this realization, in past BASS deployments, careful calibrations of the zero offsets were typically done after all the cables had been secured. In contrast, the advantage with the MAVS sensor is that it has internal, rigidly fixed wires that do not flex, and therefore its zero offset does not change as much, thereby avoiding the need to recalibrate the zero offsets (Thwaites and Williams III, 1996). In fact, a single "zero" calibration should suffice, barring dimensional changes with temperature and age. In any case, MAVS is relatively easy to "zero" because the sensor is at the end of a tube and can be immersed in a bucket of still water or a pot of hot carrageenan that is allowed to cool and gel. If MAVS is powered up while so immersed, it automatically obtains an average of 16 measurements of velocity and stores them in an array for subtraction from subsequent measurements. This is essential for doing Earth coordinate rotations with an ATT current meter (Williams III and Thwaites, 1998).

MAVS has other advantages over BASS. For example, the structural rings holding the acoustic transducers have streamlined cross-sections to reduce drag when the flow is 45° from perpendicular to the central tube, to reduce flow obstruction at this attitude, and to improve the cosine response. The geometry is simpler to make, because larger pieces of the sensor are moldable, to reduce labor and cost of production. The MAVS uses four acoustic paths of 10 centimeters to reduce sensor size and is operated by modified BASS electronics. The production version uses surface-mount technology electronics to reduce the size of the sensor electronics. The central tube is large, to allow use as the tension member in a mooring.

Reynolds stress and turbulent kinetic energy derive solely from fluctuations in velocity components (Williams III and Beckford, 1999). In the case of Reynolds stress, the mean is subtracted from the time series of velocity before the product of the downstream component with the vertical component is averaged. The average self-product of the fluctuations gives the turbulent kinetic energy, again rejecting the mean velocity. Consequently, "zero-offset" error is not a concern for these measurements. Only a very high rate of zero-offset drift would be a concern. However, for other purposes, the loss of vector truth and the loss of accuracy in speed are concerns. Thus, evaluation of performance of the instrument under various conditions that are expected in real field situations needs to be carried out.

Thwaites and Williams III (1996) reported the comparison of the measured sensor performance of BASS and MAVS for cosine response and flow noise. Williams III and Beckford (1999) reported results of additional tests of BASS and MAVS such as bucket zero, tank tests, and tow-tank tests. ATT sensors have electronic offsets in general that can only be corrected up to a point without a physical zero-point measurement. For such measurement, the sensor is placed in still fluid, such as water, seawater, gelatin, or some other stationary fluid, and a measurement is made. This becomes the zero-point calibration, and it is subtracted from all subsequent determinations of velocity. As noted earlier, BASS and MAVS both measure the vector velocity components in a cage 10 cm in diameter. The essential constructional difference between BASS and MAVS is that whereas the acoustic paths of BASS cross the center of the measurement volume, the acoustic paths of MAVS are on chords surrounding a central support. An ideal ATT current meter measures the component of flow speed along an acoustic axis. Combining several axes, three or more for a 3-D current meter, produces a flow vector. If one or more axes have a zero-point error, the resulting vector will be skewed. A 10 cm/s current with a zero-point error of 1 cm/s can have a vector direction error of 0.1 radian or 5.7°. According to Williams III (2001), the ratio of the zero-point error to the velocity is the critical determinant of this error. Because the offset is a constant, the direction error increases as the speed decreases. Cosine response measures sensitivity to off-axis velocity and any change in sensor gain with attitude relative to the flow. An ideal sensor measures the undisturbed flow, which is independent of sensor attitude. The rings in the BASS sensor appear to partially obstruct flow that is steep, thereby causing the sensor to measure less than the undisturbed flow, when the flow is more than 30° from the horizontal. Thus the BASS sensor provides good cosine response for horizontal flows but imperfect cosine response for steep flows. The BASS cosine response to steep flows is thought to be impacted by the rings. Streamlining the rings for these steep angles in the MAVS sensor reduced the flow blockage and improved the sensor's cosine response.

The measured flow noise for both BASS and MAVS has been found to be largely linear with relative velocity, as expected. Unfortunately, the MAVS sensor has a larger cylinder-diameter-to-acoustic-path length ratio, and therefore its flow noise is much larger than that of BASS. The ratio of noise was found to be consistent with the diameter over path-length ratio of Equation 9.13. In a nutshell, performance evaluation studies conducted by Thwaites and Williams III (1996) provided an indication that an ATT current meter such as MAVS, with a central strut large enough to take a mooring load, despite good cosine response to steep flow angles, will not be good at measuring small-scale turbulence due to its large ratio of strut diameter to acoustic path length. However, fairing of the transducer support rings achieved reduction of flow distortion by the sensor to an acceptable level (Williams III and Thwaites, 1998). According to them, the main error in flow-velocity measurement using acoustic current meters is loss of a received acoustic pulse. An acoustic reflector such as a large air bubble or a bone can block an acoustic path and prevent one or more components of the velocity from being measured. This is detected by requiring that both transducers defining an acoustic path have received signals by the end of the measurement interval. If either or both have not received signals, a flag word is stored in place of the velocity. This word is detected when the normal and reversed measurements are subtracted. If either the normal or the reversed measurements contains the flag word, the flag word replaces the result of subtraction. When the velocities in the sensor frame are rotated into Earth coordinates, the presence of a flag word is checked for each component of the velocity and, if it is present, the Earth coordinate velocities are all replaced by flag words.

Because the zero offset can be measured and applied as a correction, zero offsets themselves are not a problem. It is the changes in zero offset that create error. Williams III (2001) reported study of zero-offset drift of MAVS in laboratory as well as field environments. In MAVS and its predecessor, BASS, the connection of each pair of transducers to the measurement circuits is reversible with a transistor switch. The electronic circuits after the switch drift with temperature, age, and voltage variations, but these effects cancel out when two measurements are made sequentially, first with the transducers connected normally and then with the transducers connected in reverse. The results are subtracted. The drift in electronic characteristics of the cascade amplifier, voltage comparator, charge integrator, voltage follower, differential amplifier, and A/D converter are all cancelled when the second member of the pair is subtracted from the first. In extended zero tests conducted by Williams III (2001) in a bucket in the lab, the "zero" was not seen to drift. Cooling the electronics with

a circuit cooler did not have an effect either, until condensation occurred on the circuit board, degrading the insulation of the off circuits.

Three MAVS were deployed at 2,300 meters for up to three months at the Endeavour Field of the Juan de Fuca hydrothermal vents (Williams III and Tivey, 2001). Organisms covering the instruments were an interesting feature of long deployments of current meters. It was thought that these organisms might impede the flow, but fortunately they did not in this deployment.

Morrison et al. (2002) reported the development of a modified MAVS, known as MAVS3, which is the third version of MAVS. To make a measurement of the component of flow along a single acoustic axis, MAVS transmits a short pulse (15 cycles at 1.7 MHz) simultaneously from both ends of the acoustic path. The received signals are amplified in a cascade circuit and passed through a Schmitt trigger to a counter. This process provides significant immunity from noise (Williams III et al., 1987). In each receive channel, the counter detects the 15^{th} negative-going zero crossing of the received signal and switches an active current source to a capacitor that has previously been fully discharged. The two acoustic signals arrive differentially as a function of flow speed along the axis, so the integrating capacitors in the receiver channels begin charging at different times. After the arrival of the second signal, MAVS simultaneously switches both current sources away from the capacitors. The capacitor voltages are differentially amplified, and the analog difference voltage is digitized with a 12-bit analog-to-digital converter (ADC).

To further improve accuracy, each measurement is repeated with the receiver channels electrically exchanged. The results of the normal and reversed measurements are differenced in software to remove receiver bias. The result is a differential travel-time measurement, in digital form, with accuracy in time of 40 picoseconds. Over the 10 cm MAVS acoustic path length, this means a velocity accuracy of 0.05 cm/s. The full linear range of the measurement is $\pm$180 cm/s. With this level of measurement accuracy, the limiting factor becomes the disturbance of the flow created by the sensor. The sensor head was designed to minimize the distortion.

Real-time MAVS3 measurements are available to an operator as a serial stream of ASCII data using standard RS-232 or RS-485 protocols. Any generic PC with a serial port and running a simple terminal emulator can display and log MAVS3 data in real-time. The problem of facilitation of simultaneous real-time data recording from an array of multiple MAVS3 sensors without the use of multiple PCs has been well addressed by adding an analog output capability to MAVS3. The advantage of doing this was that multichannel analog-to-digital acquisition and logging systems are standard equipment in many hydrodynamics laboratories, and such systems are well suited to sampling a large array of sensors; they provide the operator with real-time datastreams that have been referenced to a common time base. The digital-to-analog conversion of MAVS3 velocity measurements provides stable analog outputs that can be sampled asynchronously by the external system. Alternatively, a "data-ready" pulse permits sampling synchronized to the MAVS3 measurement interval (Morrison et al., 2002).

9.3. ACOUSTIC DOPPLER CURRENT METER

Acoustic Doppler water-flow measurement technologies have a close similarity to the laser Doppler technologies discussed in Chapter 2, and both can measure oceanic currents remotely. The major differences between these two technologies lie in the differences in spatial resolution and the maximum achievable range for remote measurement. The considerably short wavelength of the laser beam permits flow measurements with fine spatial resolution, but large attenuation of the laser beam in water does not permit remote measurements of water currents from distances more than a meter or so away from the sensor. Whereas seawater is rather opaque to electromagnetic radiation such as laser and radio waves, it is almost transparent to the mechanical form of energy known as *acoustic radiation*. This unique property of the acoustic radiation permits the acoustic Doppler current meter to nonintrusively measure ocean currents from large distances from the sensor. This superb capability of acoustic Doppler current meters circumvents one of the major limitations of the conventional Eulerian current meters, namely obstruction of the flow field by the body of current meter and the resulting dependence of the accuracy of current measurements on the current meters' azimuthal and tilt responses, which are generally far from the ideal cosine responses.

Acoustic Doppler current meter's operation relies on the mechanism of acoustic volume scattering from a cloud of moving scatterers in the flow field and the well-known phenomenon of the Doppler effect. The term *scatterer* encompasses any kind of inhomogeneity in water, including suspended particulate matter, biological organisms, minute bubbles, and so on. These scatterers serve as passive tracers of the flow field. In operation, acoustic sonar (which is the sensor) transmits a narrow-beam acoustic pulse into the flow field in a given direction, and the Doppler shift of the volumetric echo returned from the scatterers in the flow field is used to determine the relative radial velocity of the current flow between the volume bounded by the scatterers and the sonar. If the stationary transmitter, stationary receiver, and flow velocity vector v are in the same plane, the

FIGURE 9.23 Eulerian-style Aanderaa RCM 9 MkII and RCM 11 Doppler acoustic current meters. *(Source: Aanderaa RCM 11 brochure.)*

frequency f_r of the received acoustic wave differs from the transmitted frequency f_t according to the relation (Clay and Medwin, 1977):

$$f_r = f_t\left(\frac{c + v\cos\theta_t}{c - v\cos\theta_r}\right) \tag{9.24}$$

where c is the velocity of sound in the water at rest, and θ_t and θ_r are the angles made by the flow velocity vector v with the transmitter beam and the receiver beam, respectively. For a given geometry, the Doppler shift $(f_r - f_t) = f_D$ is +ve or −ve, depending on the direction of the flow. From Equation 9.24, we get,

$$\frac{(f_r - f_t)}{(f_r + f_t)} = \frac{(v\cos\theta_t + v\cos\theta_r)}{(2c + v\cos\theta_t - v\cos\theta_r)} \tag{9.25}$$

For ocean currents, the received frequency differs only slightly from the transmitted frequency, so that $(f_r + f_t) = 2f_t$. For a symmetrical geometry, $\theta_t = \theta_r = \theta$. Based on these considerations, Equation 9.25 can be written as:

$$f_D = \frac{(2f_t v\cos\theta)}{c} \tag{9.26}$$

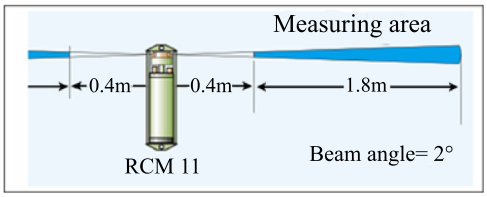

FIGURE 9.24 Illustration of the acoustic beam geometry and the active measuring window (starting at ∼0.5 m and ending at ∼2 m from the transducer) of the Aanderaa Doppler acoustic current meter. *(Source: Aanderaa manual for RCM 11 Doppler acoustic current meter.)*

If the receiving transducer is the same as the one used for transmitting the ping, then $\theta = 0$ so that Equation 9.26 gets simplified as:

$$f_D = \frac{(2f_t v_r)}{c} \tag{9.27}$$

In this expression, v_r is the radial current velocity, i.e., the component of the current speed along the acoustic transmission path.

An important factor that influences the development of acoustic Doppler current meter is the transmission frequency f_t. From Equation 9.27 it is evident that for a given flow velocity, higher transmission frequencies are desired to produce larger Doppler shifts. The transmission frequency also influences the transducer design, its weight, and its size. However, attenuation of the acoustic wave increases as the transmission frequency increases, and the choice of frequency will, therefore, be a compromise.

The backscattered signal, normally of microvolts in amplitude, is composed of the random sum of the individual scattering amplitudes, each having a Doppler frequency shift associated with the radial velocity (i.e., water-flow velocity along the acoustic beam) of the scatterer. Because the micro-inhomogeneities that cause the scattering are of random sizes, the received signal is subject to amplitude modulation. Phase incoherencies also arise as a result of different ranges of the individual scatterers from the acoustic receiver as well as their random motion due to turbulence within the defined scattering volume. The signal is also corrupted by an additive white Gaussian noise. Thus, the received signal is a highly distorted version of the transmitted signal wherein its deterministic properties are no longer valid; rather, the signal is statistical in nature with Gaussian distributions. For this reason, a realistic approach for estimation of Doppler shift information is some form of statistical methods. Most of the Doppler shift information is contained in the first and second moments of the Doppler spectrum. One method of obtaining these moments is to Fourier transform the received echoes. These can also be obtained from estimates that do not involve the Fourier transform operation.

Based on the experience gained by past researchers in Eulerian-style Doppler acoustic current meters (see Chapter 2) and taking due account of various geometries vis-à-vis their advantages and limitations, Aanderaa Instruments of Norway developed a current meter, known as the RCM 9, and subsequently its modified model, known as the RCM 11 (Figure 9.23). In these current meters, a Doppler measurement starts by sending out a pulse of acoustic energy, called a *ping*. As mentioned earlier, due to particles and bubbles in the water, a fraction of the transmitted sound is reflected backward. This echo is then picked up by a receiver, which, in the present case, is the same transducer used for transmitting the ping. The uncertainty of a single Doppler measurement is very dependent on the transmitted frequency (f_t), the length (L) of the transmit pulse (which is assumed to be the same as the length of the active measuring window) and the beam geometry, and a proportionality constant (k_b), which is dependent on beam angle and several other factors. The standard deviation of one measurement (σ_s) is expressed as:

$$\sigma_s = \left(\frac{k_b}{f_t L}\right) \tag{9.28}$$

By averaging several of these Doppler measurements, the standard deviation can be minimized. It was found that the accuracy would be acceptable by using a transmission frequency of 2 MHz, a beam angle of $\pm 2^\circ$, a measuring window of $\sim$1.5 m, and averaging 150 pings. To receive as much reflected acoustic energy as possible, the transmit pulse is set to be the same length as the measuring window. The pulse length of the ping is therefore set to 1 ms, which corresponds to a distance of 1.5 m. By measuring the incoming echo frequency from 0.67 ms to 1.67 ms after the ping is sent out, the active measuring window will start at $\sim$0.5 m and end at $\sim$2 m from the transducer (Figure 9.24). The water current velocity vector in the horizontal plane can be determined by the use of two mutually orthogonal transducers on a horizontal plane. However, to make the sensor as symmetrical as possible, Aanderaa chose to use four transducers, two opposite at each axis (see Figure 9.24). By pinging one at a time, the same electronics are used for transmitting and receiving. The circuit incorporates two switches: one for selecting one of the four transducers and the other to switch between transmitting and receiving.

When a Doppler sampling starts, the correct transducer is selected and the ping is transmitted. After the first part of the ping has traveled 0.5 m and back again, the active transducer is switched to receiver mode. The echo signal received in the receiver electronics is amplified and filtered. The signal is then mixed down to 455 KHz. This signal is then filtered and amplified until digital level is reached. The amplified signal is then fed to a programmable logic device (PLD) where the frequency is measured very accurately. Both the transmit pulse and the measurement are based on the same 20 MHz crystal oscillator. This methodology minimizes the risk of temperature influence of the measurements.

A microprocessor is used for controlling the different timing and for calculating the current velocity vectors. The main component of current in the sea is usually horizontal. Because a moored instrument is likely to be inclined, the measuring axis will not be in the horizontal plane. For this reason, the current sensor is equipped with an electrolytic tilt sensor for both axes. The acoustic transducers, a Hall effect compass, and the tilt sensors are all incorporated in one molded unit, called a Doppler current sensor. After a cycle of four pings, one in each direction, the tilt is measured and two horizontal current components are calculated. For current direction to be meaningful, these components must be referred to Earth coordinates. On the basis of the readings from the internal Hall effect compass, the two current components are converted to north and east components. These components are accumulated for each cycle of four pings. At the end of the measurement interval, the vector average of these components is calculated and sent out as current speed and current direction at the sensor output.

Most of the electronics are turned off between the Doppler samplings. This makes the average power consumption very low, almost proportional to the ping rate. The sensors are mounted on the top endplate of the instrument case, with the Doppler current sensor on a central stud. All the sensors except for the temperature are molded in polyurethane with excellent antifouling properties. The measuring interval of the instrument can be selected by setting a rotary switch on the electronic board inside the pressure tube. This board controls the ping rate so that 600 pings are taken during each measurement interval. This feature makes the accuracy independent of the measuring interval and the power consumption per measuring interval almost constant. Figure 9.25 shows typical examples of preparations for deployment of an Aanderaa Doppler acoustic current meter in the Indian Ocean.

One of the main applications of this current meter is monitoring the large-scale circulation of the oceans. Because this current meter is free of the threshold found in several mechanical sensors, weak currents such as those found in the deep oceans can be monitored more accurately and, due to the low power consumption, data can be collected for up to two years (Hovdenes, 1998).

In tropical water bodies, the upper few meters of the water column (the photic zone) are subject to severe biological fouling, which includes algal growth and heavy incrustation with barnacles and mussels. In higher latitudes, such fouling is very common during the summer season. Figure 9.26 shows an example of such fouling

FIGURE 9.25 Photographs showing preparations for deployment of the Aanderaa Doppler Acoustic Current Meter in the Indian Ocean. *(Source: Courtesy of Dr. Sanil Kumar, National Institute of Oceanography, Goa, India.)*

that occurred on a deployment at the Gulf of Maine. The Doppler acoustic current meter has no moving parts, and it is immune to even the severe fouling and mooring motion that plague mechanical current meters under these conditions. Aanderaa's proprietary forward-pinging algorithm especially assures that the data are collected upstream and free from contamination from the instrumental wake.

FIGURE 9.26 Photograph showing severe biological fouling on the Aanderaa RCM 9 MkII Acoustic Doppler Current meter deployed at the Gulf of Maine and still giving reliable data. *(Source: Aanderaa magazine Sensors & Systems, No. 21, p. 1–4, June 2004.)*

REFERENCES

Abernathy, F.H., Kronauer, R.E., 1962. The formation of vortex streets. J. Fluid Mech. 13, 1–20.

Appell, G.F., 1978. A review of the performance of an acoustic current meter. In: Woodward, W., Mooers, C.H.K., Jensen, K. (Eds.), Proc. Working Cong. on Current Measurement. Tech. Rep. DEL-SG-3-78 University of Delaware, Newark, DL, USA, pp. 35–58.

Appell, G.F., 1979. Performance assessment of advanced ocean current sensors. IEEE J. Oceanic Eng. OE-4 (1), 1–4.

Aubrey, D.G., Trowbridge, J.H., 1985. Kinematic and dynamic estimates from electromagnetic current meter data. J. Geophys. Res. 90, 9137–9146.

Bernier, R.N., Brennen, C.E., 1983. Use of the electromagnetic flow meter in a two-phase flow. International Journal of Multiphase Flow 9 (3), 251–257.

Bevir, M.K., 1970. The theory of induced voltage electromagnetic flow meters. J. Fluid Mech 43 (3), 577–590.

Bivins, L.E., 1975. Turbulence effects on current measurement. M.S. thesis. University of Miami, Coral Gables, FL, USA.

Blanton, J.O., Lin, G., Elston, S.A., 2002. Tidal current asymmetry in shallow estuaries and tidal creeks. Continental Shelf Research 22, 1731–1743.

Blevins, R.D., 1977. Flow-induced vibration. Van Nostrand.

Bowden, K.F., Fairbairn, L.A., 1956. Measurements of turbulent fluctuations and Reynolds' stresses in a tidal current. Proc. R. Soc. (A) 237, New York, NY, USA. 422–438.

Brown, N.L., 1992. A simple low-cost acoustic current meter, Vol. 2. Proc. Oceanology International '92, Brighton, UK. March 10–13.

Clay, C.S., Medwin, H., 1977. Doppler effects for moving objects, sea surface and ships. In: Acoustical oceanography: Principles and applications. Wiley Interscience, John Wiley & Sons Singapore Pte. Ltd., Singapore, pp. 334–338.

Clayson, C.H., 1983. A vector averaging electromagnetic current meter for near-surface measurement. In: Proc. IEEE Third Working Symposium on Oceanographic Data Systems. IEEE Computer Society, New York, NY, USA, pp. 81–87.

Collar, P.G., 1993. A review of observational techniques and instruments for current measurements from the open sea. Report No. 304, Institute of Oceanographic Sciences, Deacon Laboratory, Godalming, Surrey, United Kingdom.

Collar, P.G., Hunter, C.A., Perrett, J.R., Braithwaite, A.C., 1988. Measurement of near-surface currents using a satellite-telemetering buoy. Journal of the Institution of Electronic & Radio Engineers 58, 258–265.

Cushing, V., 1976. Electromagnetic water current meter. Proc. Oceans '76, MTS-IEEE Conference. IEEE, Washington, DC, USA, September 1976.

Desa, E.S., Desa, E., 1980. A closed-loop electromagnetic flow meter. J. Phys. E: Sci. Instrum. 13, 233–235.

Grant, W.D., Williams III, A.J., Gross, T.F., 1985. A description of the bottom boundary layer at the HEBBLE site: low-frequency forcing, bottom stress and temperature structure. Mar. Geol 66, 219–241.

Griffiths, G., 1979. The effect of turbulence on the calibration of electromagnetic current sensors and an approximation of their spatial response. Institute of Oceanographic Sciences Report No. 68, Godalming, Surrey, United Kingdom.

Griffiths, G., Collar, P.G., Braithwaite, A.C., 1978. Some characteristics of electromagnetic current sensors in laminar flow conditions. Institute of Oceanographic Sciences Report No. 56, Godalming, Surrey, United Kingdom.

Gytre, T., 1976. The use of a high sensitivity ultrasonic current meter in an oceanographic data acquisition system. Radio and Electronic Engineer 46, 617–623.

Gytre, T., 1980. Acoustic travel time current meters. In: Dobson, F., Hasse, L., Davis, R. (Eds.), Air-sea interaction: Instruments and methods. Plenum Press, New York, NY, USA, pp. 155–170.

Hovdenes, J., 1996. The RCM 9: A unique new instrument for measuring ocean currents and other oceanographic parameters. Proc. Oceans '96 Conference Vol. 1. Issue 1 (revised January 1998).

Jones, I.S.F., 1980. Electromagnetic current meters. In: Dobson, F., Hasse, L., Davis, R. (Eds.), Air-sea interaction: Instruments and methods. Plenum Press, New York, NY, USA, pp. 219–229.

Joseph, A., 1981. Electromagnetic flow meter. NIO Technical Report, Dona Paula, Goa, India, pp. 1–22.

Kanwisher, J., Lawson, K., 1975. Electromagnetic flow sensors. Limnology & Oceanography, Alberta, Canada, 174–182.

Kun, A.L., Fougere, A.J., 1997. New wave direction and spectrum measurement technique. Proc. Third International Symposium on Ocean Wave Measurement and Analysis. Virginia Beach, VA, USA, Nov. 3–7, 1997, 1278–1281.

Kun, A.L., Fougere, A.J., 1998. Applications of an acoustic current measurement technique. Ocean News and Technology. September/October 1998, 36–37.

Kun, A.L., Fougere, A.J., 1999. A new low-cost acoustic current meter design. Proc. IEEE 1999, 150–154.

Lawson, K.D., Lessieux, B.J., Luck, J.M., Woody, D.C., 1983. The development of a spherical electromagnetic current meter. Proc. IEEE Oceans '83 Conference. New York, NY, USA, 187–193.

Lowell Jr., F.C., 1979. Acoustic flow meters for pipeline flow rate. Water Power & Dam Construction, 39–46.

McCullough, J.R., 1980. Survey of techniques for measuring currents near the ocean surface. In: Dobson, F., Hasse, L., Davis, R. (Eds.), Air-sea interaction: Instruments and methods. Plenum Press, New York, NY, USA, pp. 105–126.

McCullough, J.R., Graper, W., 1979. Moored acoustic travel time (ATT) current meters: Evolution, performance and future design. Woods Hole Oceanographic Institution Report No. WHOI-79-92, Woods Hole, MA, United States.

Morrison III, A.T., Williams III, A.J., Waterbury, A.C., Tierney, C.M., 2002. Analog output from a differential travel-time current meter. IEEE Oceans '02, 708–712.

Morrison III, A.T., Williams III, A.J., Martini, M., 1993. Calibration of the BASS acoustic current meter with carrageenan agar. Proc. Oceans '93, IEEE/OES Vol. III, 143–148.

Mulcahy, M., 1978. A solid state water current meter for wave direction sensing. Sea Technol. July 1978.

Olson, J.R., 1972. Two-component electromagnetic flow meter. Marine Technology Society Journal 6 (1), 19–24.

Sanford, T.B., Flick, R.E., 1975. On the relationship between transport and motional electric potentials in broad, shallow currents. Journal of Marine Research 33, 123–139.

Saunders, K.D., 1980. , Horizontal response of the NBIS acoustic current meter. Proc. Oceans '80. Seattle, WA, USA, September 8–10, 1980, 220–225.

Shercliff, J.A., 1962. The theory of electromagnetic flow measurement. Cambridge University Press, Cambridge, United Kingdom.

Sorrell, F.Y., Curtin, T.B., Feezor, M.D., 1990. An electromagnetic current meter-based system for application in unsteady flows. IEEE J. Oceanic Eng 15 (4), 373–379.

Sorrell, F.Y., Curtin, T.B., Feylor, M.D., 1985. Electromagnetic shear flow meter for remote oceanic applications. U.S. Patent # 4543822.

Thorpe, S.A., Collins, E.P., Gaunt, D.I., 1973. An electromagnetic current meter to measure turbulent fluctuations near the ocean floor. Deep-Sea Res 20, 933–938.

Thwaites, F.T., Williams 3rd, A.J., 1996. Development of a modular acoustic velocity sensor. Proc. Oceans '96, 607–612.

Trivett, D.A., Terray, E.A., Williams III, A.J., 1991. Error analysis of an acoustic current meter. IEEE J. Ocean. Eng 16 (4), 329–337.

Tucker, M.J., Smith, N.D., Pierce, F.E., Collins, E.P., 1970. A two-component electromagnetic ship's log. J. Inst. Navig. 23, 302–316.

Urick, R.J., 1975. Propagation of sound in the sea: transmission loss, I. In: Principles of underwater sound. McGraw-Hill, Columbus, OH, United States, pp. 93–135.

Wang, J.Z., Tian, G.Y., Simm, A., Lucas, G.P., 2008. Simulation of magnetic field distribution of excitation coil for EM flow meter and its validation using magnetic camera. In: 17th World Conference on Nondestructive Testing. Shanghai, China, Oct. 25–28, 2008.

Wang, J.Z., Tian, G.Y., Lucas, G.P., 2007. Relationship between velocity profile and distribution of induced potential for an electromagnetic flow meter. Flow Measurement and Instrumentation 18, 99–105.

Williams III, A.J., 1985. BASS, an acoustic current meter array for benthic flow-field measurements. Mar. Geol 66, 345–355.

Williams III, A.J., 1995. Linearity and noise in differential travel time acoustic velocity measurement. Proc. IEEE Fifth Working Conference on Current Measurement, IEEE/OES. Feb. 7–9, 1995, 216–221.

Williams III, A.J., 2001. Acoustic current meter zero offset drift. Proc. IEEE Oceans '01, 916–921.

Williams III, A.J., Beckford, C., 1999. Reynolds stress resolution from a Modular Acoustic Velocity Sensor. Oceans '99, 386–390.

Williams III, A.J., Thwaites, F.T., 1998. Earth coordinate 3-D currents from a modular acoustic velocity sensor. Proc. IEEE Oceans '98, 244–247.

Williams III, A.J., Tivey, M.K., 2001. Tidal currents at hydrothermal vents, Juan de Fuca Ridge. Sea Technology. June 2001, 62–64.

Williams III, A.J., Tochko, J.S., Koehler, R.L., Grant, W.D., Gross, T.E., Dunn, C.V.R., 1987. Measurement of turbulence in the oceanic bottom boundary layer with an acoustic current meter array. J. Atmos. Oceanic Tech 4 (2), 312–327.

Woodward, W.E., Appell, G.F., 1973. Report on the evaluation of a vector averaging current meter. NOAA Technical Memorandum NOAA-TM-NOS-NOIC-1. pp. 13–16.

BIBLIOGRAPHY

Chriss, T.M., Caldwell, D.R., 1982. Evidence for the influence of form drag on bottom boundary layer flow. J. Geophys. Res. 87, 4148–4154.

Cushing, V., 1976. Electromagnetic water current meter, Paper 25C. Proc. MTS-IEEE Oceans '76 Conference. IEEE, 1976; 25C-1-25C-17, Washington, DC, USA, Sept. 13–15, 1976.

Hardies, C.E., 1975. An advanced two-axis acoustic current meter. Proc. Offshore Technology Conference II, 465–476.

Heldebrandt, K.E., Trest, L.S., Michelena, E.D., 1978. The development and testing of current meters for long-term deployment on the continental shelf. Proc. Oceans '78. Washington, DC, USA, 308–314.

Lawson, K.D., Brown, N.L., Johnson, D.H., Mattey, R.A., 1976. A three-axis acoustic current meter for small scale turbulence. ISA, 501–508.

Morrison, A.T., Williams III, A.J., Martini, M., 1993. Calibration of the BASS acoustic current meter with carrageenan agar. Proc. Oceans '93, 143–148.

Robbins, R.J., Morrison, G.K., 1981. Acoustic direct reading current meter. Proc. IEEE Oceans '81 Conference, 506–511.

Thwaites, F.T., Williams, A.J., 2001. BASS measurements of currents, waves, stress and turbulence in the North Sea bottom-boundary layer. IEEE J. Oceanic Eng 26, 161–170.

Trivett, D.A., Williams, A.J., 1994. Effluent from diffuse hydrothermal venting. 2. Measurements of plumes from diffuse hydrothermal vents at the southern Juan de Fuca Ridge. J. Geophys. Res 99, 18417–18432.

Wang, J.Z., Lucas, G.P., Tian, G.Y., 2007. A numerical approach to the determination of electromagnetic flow meter weight functions. Measurement Science and Technology 18 (3), 548–554.